

UNCLASSIFIED

| |
|--|
| |
| |
| |
| AD NUMBER |
| AD907851 |
| NEW LIMITATION CHANGE |
| TO Approved for public release, distribution unlimited |
| FROM Distribution authorized to U.S. Gov't. agencies only; Test and Evaluation; Sep 1972. Other requests shall be referred to the Air Force Armament Laboratory, Attn: DLJC, Eglin AFB, FL 32542. |
| AUTHORITY |
| USADTC ltr, 14 Mar 1979 |

THIS PAGE IS UNCLASSIFIED

①

AFATL-TR-72-179

AD 907851

MK82 BALLUTE RETARDER SYSTEM

GOODYEAR AEROSPACE CORPORATION

B

TECHNICAL REPORT AFATL-TR-72-179

**AD No. _____
DDC; FILE COPY**

1473

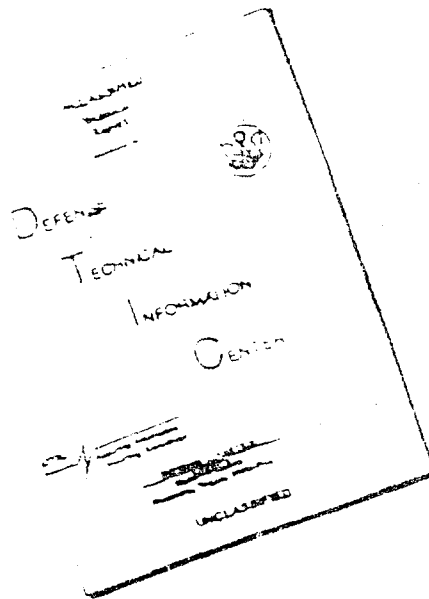
SEPTEMBER 1972

DDC
RECEIVED
6 1972
E

Restrictions limited to U. S. Government agencies only; this report contains test and evaluation; distribution unlimited until September 1972. Other requests for this report will be referred to the Air Force Research Laboratory (AFRL) at Eglin Air Force Base, Florida 32115.

| | |
|------------------------------------|--|
| ACCESSION # | |
| NTS | EX-100 Section <input type="checkbox"/> |
| DDC | EX-100 Section <input checked="" type="checkbox"/> |
| UNANNOUNCED | <input type="checkbox"/> |
| JUSTIFICATION | <input type="checkbox"/> |
| BY | |
| DISTRIBUTION RESPONSIBILITY OFFICE | |
| Date of receipt | |

DISCLAIMER NOTICE



THIS DOCUMENT IS BEST
QUALITY AVAILABLE. THE COPY
FURNISHED TO DTIC CONTAINED
A SIGNIFICANT NUMBER OF
PAGES WHICH DO NOT
REPRODUCE LEGIBLY.

REPRODUCED FROM
BEST AVAILABLE COPY

MK82 Ballute Retarder System

N. T. Kareffa

Distribution limited to U. S. Government agencies only; this report documents test and evaluation; distribution limitation applied September 1972. Other requests for this document must be referred to the Air Force Armament Laboratory (DLJC), Eglin Air Force Base, Florida 32542.

FOREWORD

This report was prepared by ^{new} Goodyear Aerospace Corporation, Akron, Ohio, under Contract F08635-72-C-0096 with the Air Force Armament Laboratory, Eglin Air Force Base, Florida. The report covers the period from 1 January 1972 through 30 September 1972. Lieutenant Page G. McGirr (DLJC) was program monitor for the Armament Laboratory.

The contractor's report number is GER-15693. Contractor personnel contributing to this report were A. C. Aebischer, Recovery Systems Engineering Department; N. T. Karaffa, project engineer; S. A. Weinberg, aerodynamic analysis; J. F. Houmard, fabric structural analysis; R. A. Yurick, Mechanical structural analysis; and E. L. Fargo, test operations.

This technical report has been reviewed and is approved.



FENDRICK J. SMITH, Colonel, USAF
Chief, Fuzes and Munition Control Systems Division

ABSTRACT

Two retarder systems for the MK82, utilizing ram-air inflated Ballutes, were designed, developed, fabricated, and tested. One system was designed for MK82 mine application and the other system for MK82 general purpose bomb application. Ballistic characteristics of the MK82 general purpose system in the low drag mode are to be comparable to the MK82/MAU-93 and in the high drag mode to be comparable to the MK82/MK15. The system is to function in association with MAU-146 timer, FMU-54 fuze, and ATU-35 drive assembly. Basic technical disciplines presented herein are design, aerodynamic analysis, and structural analysis. Vibration test results are also presented. Both types of systems were delivered for flight testing and system feasibility testing by the Armament Development and Test Center.

Distribution limited to U. S. Government agencies only; this report documents test and evaluation; distribution limitation applied September 1972. Other requests for this document must be referred to the Air Force Armament Laboratory (DLJC), Eglin Air Force Base, Florida 32542.

TABLE OF CONTENTS

| Section | Title | Page |
|---------|---|------|
| I | INTRODUCTION. | 1 |
| II | DESIGN REQUIREMENTS | 3 |
| | 1. General | 3 |
| | 2. Objectives. | 4 |
| III | SYSTEM CONFIGURATIONS | 6 |
| | 1. General | 6 |
| | 2. System Configuration. | 6 |
| | a. Clamp Assembly (P/N 3113300-001-101). | 6 |
| | b. Canister Assembly (P/N 3113200-005-101) | 7 |
| | c. Aerodynamic Decelerator | 9 |
| IV | AERODYNAMIC ANALYSES. | 13 |
| | 1. Stability of the MK82 Bomb with a Ballute Canister. | 13 |
| | 2. Design Loads for the 3/4 Caliber Tail Panel and for the 1-1/2 Caliber Tail Panel. | 14 |
| | 3. Ballute Pressure Distribution | 15 |
| | 4. Ballute Drag Coefficient. | 16 |
| | 5. Design Loads for 41-Inch Ballute and Canister | 16 |
| | 6. MK82 Bomb/Ballute Terminal Velocities. | 18 |
| | 7. Effect of Mach Number on Stability. | 19 |
| | 8. Effect of Roll Attitude on Static Stability | 22 |
| | 9. Dynamic Stability Considerations. | 24 |
| | 10. Conclusions and Recommendations | 24 |
| V | STRUCTURAL ANALYSIS | 26 |
| | 1. General | 26 |
| | 2. Fabric Analysis | 26 |
| | a. Dynamic Stresses During Ballute Deployment | 26 |
| | b. Symmetrical Steady-State Stresses | 36 |
| | 3. Metal Analysis. | 48 |
| | a. General | 48 |
| | b. Loads | 48 |
| | c. Analysis. | 49 |
| VI | VIBRATION TESTS | 74 |
| | 1. General | 74 |
| | 2. Test Procedure. | 74 |
| | a. Introduction. | 74 |
| | b. Transverse Axis Number 1 Tests. | 74 |
| | c. Transverse Axis Number 2 Tests. | 74 |
| | d. Longitudinal Axis Tests | 77 |
| | 3. Test Results. | 77 |
| | a. Transverse Axis Number 1 Tests. | 77 |
| | b. Transverse Axis Number 2 Tests. | 79 |
| | c. Longitudinal Axis Tests | 79 |
| | 4. Conclusions | 81 |

TABLE OF CONTENTS (Concluded)

| Section | Title | Page |
|---------|---|------|
| VII | CONCLUSIONS AND RECOMMENDATIONS | 82 |
| | 1. Conclusions | 82 |
| | 2. Recommendations | 82 |
| | REFERENCES | 83 |

LIST OF FIGURES

| Figure | Title | Page |
|--------|---|------|
| 1 | Bomb Flight Profile With and Without Additional Aerodynamic Drag. | 2 |
| 2 | MK82 Retarder System Components. | 2 |
| 3 | MK82 Staging | 3 |
| 4 | Clamp Assembly. | 6 |
| 5 | Ballute Canister. | 7 |
| 6 | Release Assembly. | 8 |
| 7 | MK82 Ballute Descriptive Details | 9 |
| 8 | MK82 Low-Drag Configuration. | 11 |
| 9 | MK82 GP Bomb High-Drag Configuration | 11 |
| 10 | MK82 Mine Device High-Drag Configuration..... | 12 |
| 11 | Estimated Variation of Center of Pressure at Low Subsonic Velocities - MK82/Ballute Canister. | 13 |
| 12 | Estimated Pressure Distribution - 41-Inch Ballute | 16 |
| 13 | Estimated Variation of Ballute Incremental Drag | 17 |
| 14 | Estimated Variation of Drag Coefficients. | 18 |
| 15 | Estimated Variation of Normal Force Coefficient | 20 |
| 16 | Estimated Variation of Pitching Moment Coefficient | 20 |
| 17 | Estimated Variation of Static Margin with Mach Number. | 21 |
| 18 | Variation of Static Margin with Mach Number and Roll Attitude - MK82/MAU-93. | 22 |
| 19 | Variation of Static Margin with Mach Number and Roll Attitude - MK82/NOL Tail. | 23 |
| 20 | Variation of Static Margin with Mach Number and Roll Attitude - M-117 Bomb. | 23 |

LIST OF FIGURES (Continued)

| Figure | Title | Page |
|--------|--|------|
| 21 | Longitudinal Extraction of the Uninflated Ballute | 27 |
| 22 | Typical Stress-Strain Curve for High Tenacity Nylon Filament Yarns. | 29 |
| 23 | Radial Expansion of the Inflating Ballute | 31 |
| 24 | Equatorial, Fabric Hoop at an Intermediate Stage of Inflation. | 32 |
| 25 | Pressure Increase | 33 |
| 26 | Unit Area of an Equatorial, Fabric Hoop | 35 |
| 27 | Stress-Strain Curve for the 1050 Pounds Per Inch Fabric (29-Inch Diameter Ballute) | 36 |
| 28 | Meridian Profile and Pressures for the 41-Inch Ballute | 38 |
| 29 | Ballute Profile Showing Principal Radii of Curvature | 44 |
| 30 | Cross Section of Canister Shell at Access Holes . | 52 |
| 31 | Location of the Normal Force, F_N | 53 |
| 32 | Section of Aft Canister Ring and Applied Shear Load. | 57 |
| 33 | Equivalence Between Radially Loaded Cylinder and Ring. | 59 |
| 34 | Critical Stressed Area of the Forward Joint . . . | 61 |
| 35 | Critical Stressed Area of the Clamp Ring. | 65 |
| 36 | Free Body Diagrams in the Plane of the Clamp Band. | 67 |
| 37 | Free Body of Bend in the Clamp Band, Gussets Omitted | 69 |
| 38 | Free Body of Bend in the Clamp Band, Gussets Included. | 70 |
| 39 | Section Properties of the Gusseted Band Area. . . | 71 |
| 40 | Vibration Instrumentation and Transverse Axis Number 1 Installation | 75 |

LIST OF FIGURES (Concluded)

| Figure | Title | Page |
|--------|---|------|
| 41 | Transverse Axis Number 1 Installation | 75 |
| 42 | Transverse Axis Number 2 Installation | 76 |
| 43 | Transverse Axis Number 2 Installation | 76 |
| 44 | Longitudinal Axis Installation. | 77 |

LIST OF TABLES

| Table | Title | Page |
|-------|---|------|
| I | Principal Meridian Stresses and Margins of Safety | 39 |
| II | Summation of Drag on the Forward Burble Fence Surface | 40 |
| III | Summation of Drag on the Forward Ballute Surface. | 43 |
| IV | Summary of the Calculated Margins of Safety for the Metal Components. | 49 |
| V | Vibration Test Equipment. | 78 |
| VI | Test Data - Transverse Axis Number 1. | 80 |
| VII | Test Data - Transverse Axis Number 2. | 80 |
| VIII | Test Data - Longitudinal Axis | 81 |

SECTION I

INTRODUCTION

Aerial delivery of general purpose bombs is sometimes accomplished from aircraft flying at low altitudes. These low-altitude-delivered bombs are provided with high aerodynamic drag devices. The purpose of the high drag device is to decelerate the bomb to (1) insure sufficient distance between the aircraft and the exploding bomb, (2) improve accuracy by eliminating ricocheting or glancing rebound of the bomb due to a low impact angle with the ground, (3) obtain maximum effectiveness of the bomb by causing a high impact angle, and (4) control the impact velocity so that proper fuze functioning and proper ground penetration are achieved. Figure 1 depicts the flight profile of a bomb with and without a high drag device.

Current delivery of the MK82 general purpose (GP) 500-pound bomb configured with a MK15 high drag retarder is limited structurally to a low speed aircraft release. Furthermore, cases of marginal aerodynamic stability have been reported during delivery of MK82 GP bombs configured with MAU-93 low drag fins. Also, improvements are needed in delivery of the MK82 mine device configured with a MK15 retarder since this configuration could leave a tell-tale signature after impact in the form of broken retarder arms. A candidate to enhance aerial delivery of the MK82 GP bomb and mine device is a ram air-inflatable decelerator called a Ballute¹ (BALloon parachUTE). Accordingly, two retarder systems incorporating the Ballute were designed and developed. Ten MK82 GP bomb retarder systems and ten MK82 mine device retarder systems were fabricated and delivered to the Air Force for flight testing to determine feasibility of the systems. The basic components of the developed system are presented in Figure 2.

The report gives the performance goals, development design, and engineering data utilized and derived during this task. The basic technical disciplines presented are design, aerodynamic analysis, and structural analysis. Vibration test results are also presented.

¹T. M., Goodyear Aerospace Corporation, Akron, Ohio 44315

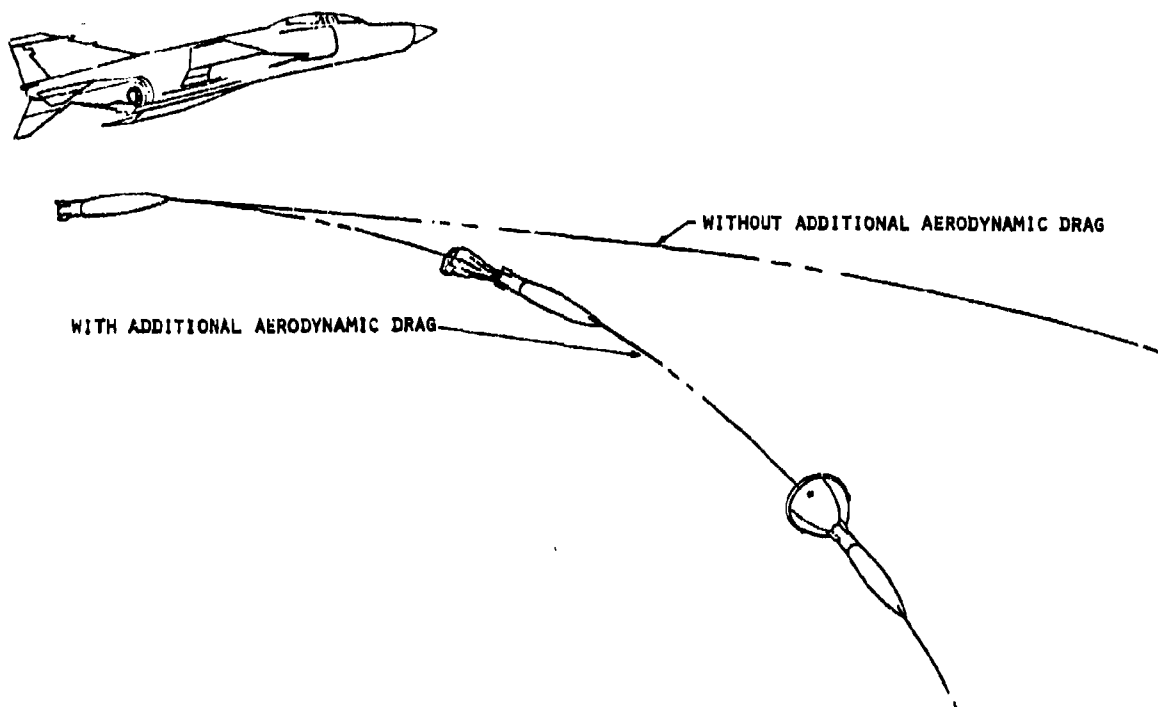


Figure 1. Bomb Flight Profile With and Without Additional Aerodynamic Drag

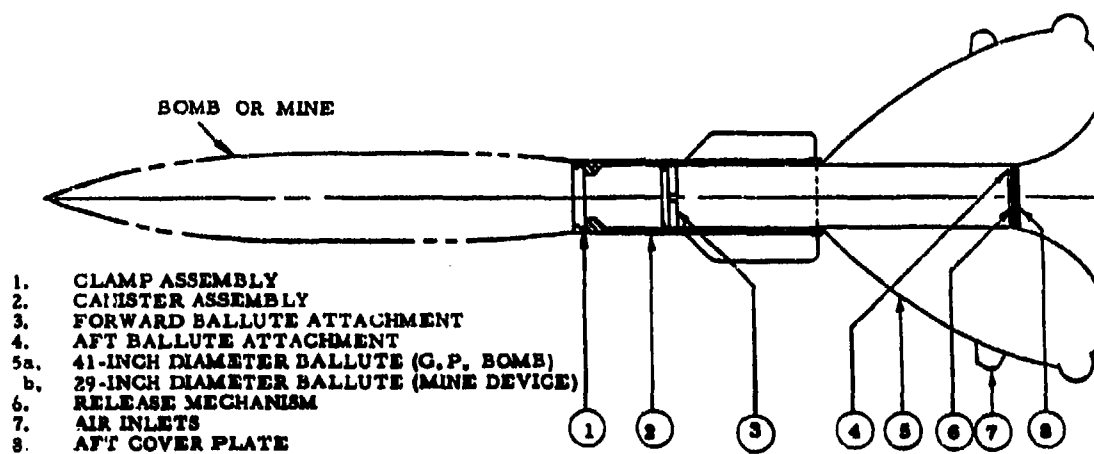


Figure 2. MK82 Retarder System Components

SECTION II
DESIGN REQUIREMENTS

1. GENERAL

Under USAF Contract FO8635-72-C-0096 with the Air Force Armament Laboratory (AFATL), the contractor was to design, fabricate, test, and deliver twenty Ballute retarder systems. The systems were for flight test evaluation to determine feasibility. The retarder system was to consist of an aerodynamic canister assembly, a ram air-inflated aerodynamic decelerator, and a clamp assembly as depicted in Figure 2.

These systems are to be capable of providing ballistic flight control by functioning in both the low aerodynamic drag mode and in the high aerodynamic drag mode. The low-drag mode will be fin stabilized. The high-drag mode will be achieved by deploying the ram air-inflated Ballute. These modes are depicted in Figure 3.

A system having the capability of functioning in either the low or high-drag modes will enhance the low altitude delivery of GP bombs.

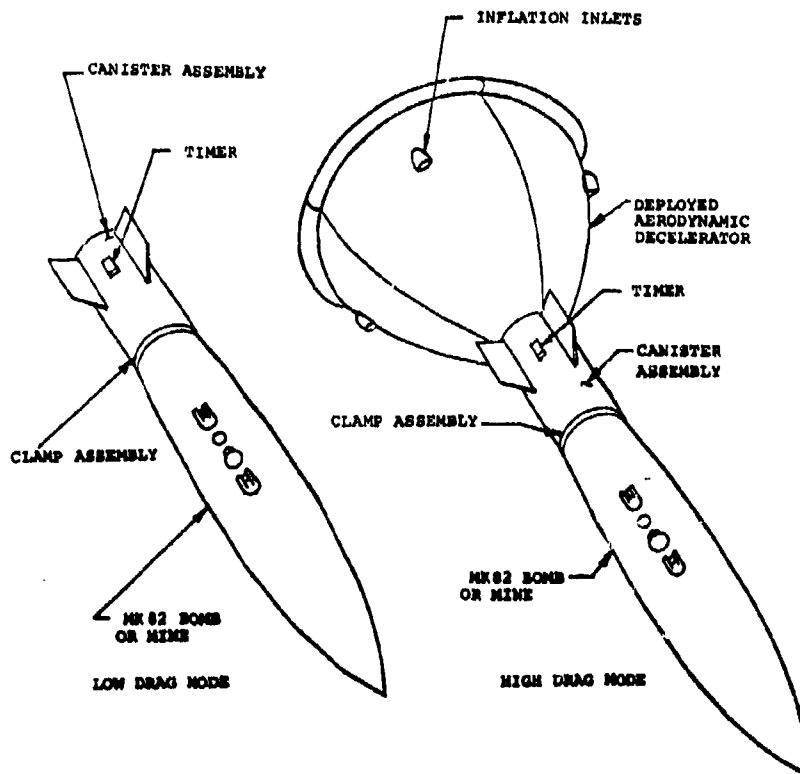


Figure 3. MK82 Staging

2. OBJECTIVES

The Ballute retarder systems were to be designed for use with the MK82 general purpose (GP) 500-pound bomb and with the MK82 mine device. These systems were to have the following performance goals:

- (1) MK82 GP Bomb Retarder System
 - (a) The retarder system will have the capability for both low and high drag modes.
 - (b) The terminal velocity for the MK82 GP bomb will be approximately 238 feet per second with the retarder system in the high-drag mode.
 - (c) The aerodynamic characteristics of the MK82 GP bomb with the retarder system in the low-drag mode will be equal to or better than the aerodynamic characteristics of the MK82 GP bomb with the MAU-93 fin.
 - (d) The deployed Ballute shall produce sufficient deceleration loads (more than 4 g's for more than 0.6 seconds) so as to be compatible with arming requirements of the FMU-54/B fuze.
 - (e) The low-drag configuration is to be the same as that used for the mine device.
- (2) MK82 Mine Device Retarder System
 - (a) The retarder system will have the capability for both low and high-drag modes.
 - (b) The terminal velocity for the MK82 mine device will be approximately 400 feet per second with the retarder system in the high-drag mode.
 - (c) There will be burial of the retarder system so that detection of the planted mine is minimized by the absence of debris at the impact point.

The design conditions for both retarder systems were:

- (1) Case 1 - Tail Panel (Fin) - Mach 1.3 at an altitude of 10,000 feet and at an angle of attack of ± 20 degrees. This requirement represents the maximum release conditions for the system without retarder deployment anticipated for future Air Force requirements.
- (2) Case 2 - Clamp Assembly - Mach 0.9 at an altitude of 250 feet and at an angle of attack of ± 20 degrees. This requirement represents the maximum release conditions for the system with retarder deployment anticipated during this flight test program.

- (3) Case 3 - Ballute - Mach 1.1 at an altitude of 2,000 feet and at a 0 degree angle of attack. This requirement represents the maximum deployment condition for the retarder design. It represents a free-fall drop from 35,000 feet altitude based on contractor estimated aerodynamic data.

SECTION III
SYSTEM CONFIGURATIONS

1. GENERAL

The configuration of the retarder systems for the MK82 GP bomb and for the MK82 mine device is essentially the same and is shown in Figure 2. The only basic difference is the size and construction of the aerodynamic decelerator or Ballute. This section describes design features of these configurations. The aerodynamic and structural analyses associated with these design features are presented in subsequent sections.

2. SYSTEM CONFIGURATION

The system consists of a clamp assembly, a canister assembly, and an aerodynamic decelerator. Details of the components are as follows:

a. Clamp Assembly (P/N 3113300-001-101)

The purpose of this clamp assembly, shown in Figure 4, is to attach the canister assembly to the GP bomb or mine device. It incorporates an indexing pin for orienting the fins on the canister with the suspension lugs on the bomb. This orientation is accomplished by inserting the pin into one of the sixteen equally spaced holes located in the aft surface of the bomb and inserting the other end into the hole located on the front face of the canister.

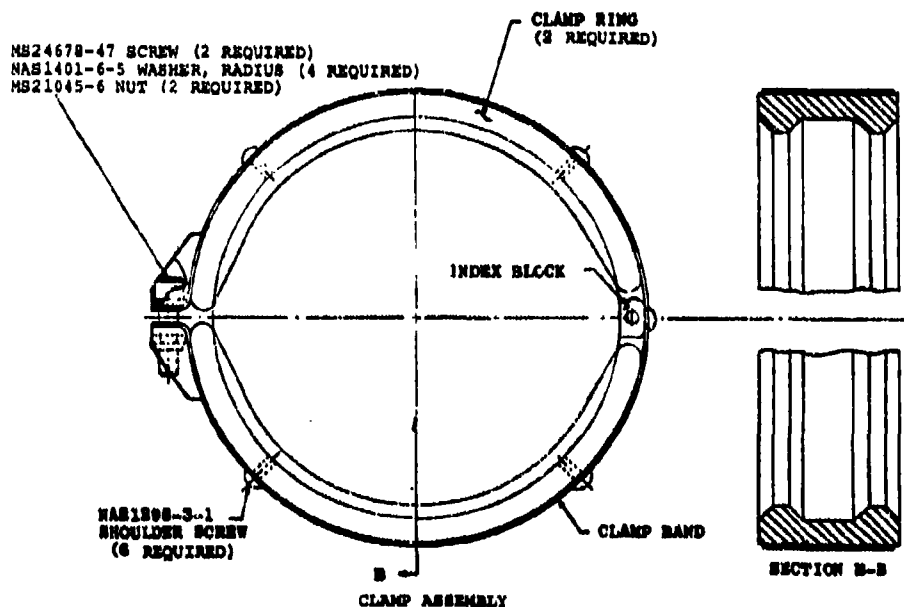


Figure 4. Clamp Assembly

As shown in Figure 4, this assembly consists of two halves of a clamp ring, a 4130 steel clamp band and an indexing block.

The two halves of the clamp ring are contoured to mate with the aft end of the bomb and with the forward end of the canister. The steel clamp band holds the two halves of the clamp ring in their mated position.

Structurally the clamp assembly transmits all flight loads to and from the bomb and the canister. Included in these flight loads are deployment, deceleration, and stabilization loads developed by the aerodynamic decelerator.

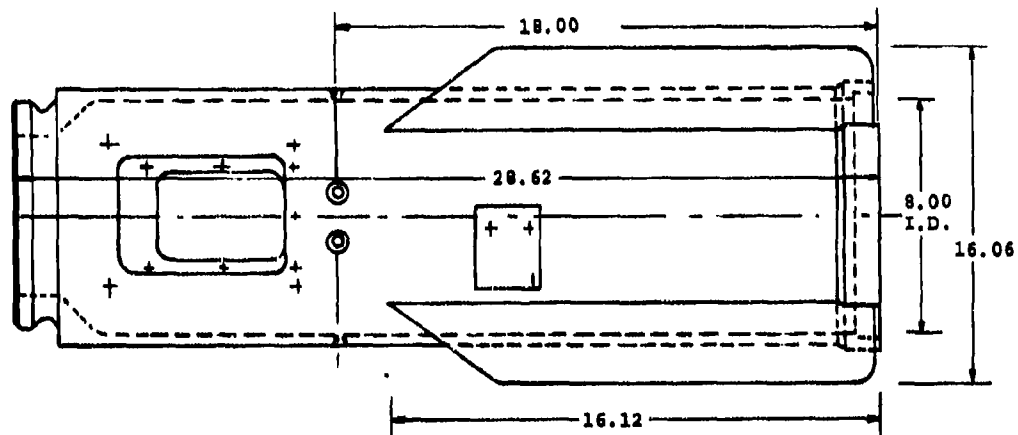
The calculated weight of this assembly is 12.63 pounds.

b. Canister Assembly (P/N 3113200-005-101)

The canister assembly consists of a Ballute canister, forward Ballute attachment, and a release mechanism.

The cylindrical Ballute canister, shown in Figure 5, is an aluminum casting with four stabilizer fins. A 365 aluminum alloy is used in this casting.

The finned canister, when attached to the bomb, forms the low drag configuration. The front end of the canister is contoured to mate with the clamp assembly. The forward section incorporates mounting provisions for the ATU-35 drive assembly device and an access panel for servicing the bomb's tail



NOTE: ALL DIMENSIONS IN INCHES

Figure 5. Ballute Canister

fuze. The middle portion includes mounting provisions for the forward Ballute clamp and for the MAU-146/B timer. The aft end of the canister is configured to accept the release mechanism. The canister is capable of containing either Ballute in the stowed configuration. Aerodynamically, the canister provides stability during low-drag mode. Structurally, the canister protects the stowed Ballute, retains the deployed Ballute, and transfers the aerodynamic drag load from the deployed Ballute to the bomb. The 29-inch-long canister weighs 34.4 pounds with access and ATU-35 provisions; and 37.0 pounds without these provisions.

The forward Ballute attachment (P/N 3113600-002-11) consists of two halves of a metal band. The forward end of the Ballute is clamped between these halves and the canister. All the aerodynamic drag load is transmitted from the Ballute through this clamp to the canister.

The release mechanism (P/N 3113600-002-101) is a spring-loaded device shown in Figure 6. The release mechanism acts as a closure to the empty Ballute canister or as a release when a retarder is used. The mechanism is retained in the canister at three equally spaced points by two drive lock pins and one machined slot. When released, the mechanism is pulled rearward by aerodynamic base drag causing deployment of the Ballute.

The release assembly incorporates the aft Ballute attachment which enables the Ballute to assume its tuck-back shape. The tuck-back shape is achieved by restraining the rearward movement of the aft cover plate and Ballute aft assembly with a center tube.

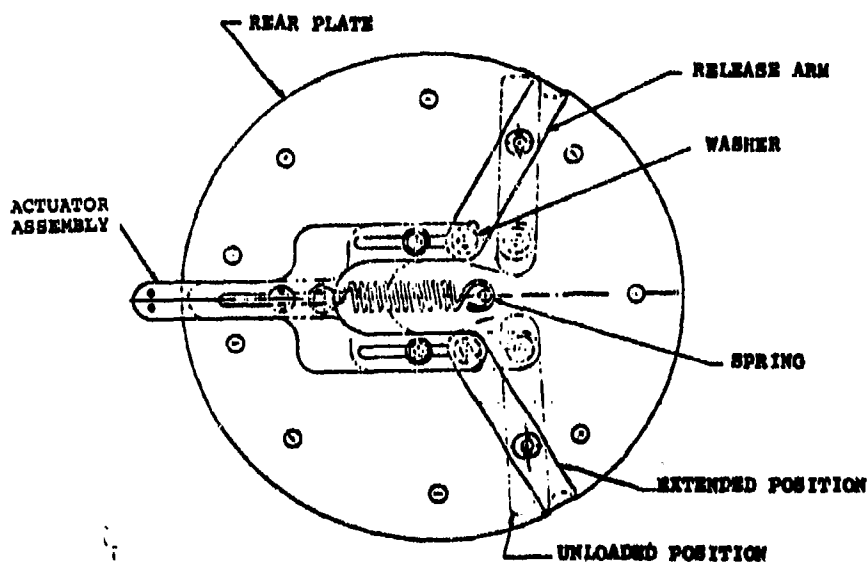


Figure 6. Release Assembly

c. Aerodynamic Decelerator

The aerodynamic decelerator design concept is essentially the same for the GP bomb as it is for the mine device. The profile, method of construction, and attachments are generally the same. The only difference between the two designs is the inflated size; therefore, the structural requirement for the fabric is also different. The type of aerodynamic decelerator used in this design is a ram air-inflated device called a Ballute (P/N 3113400-001-107) and is shown in Figure 7. The basic components of the Ballute are the center tube, Ballute, burble fence, and air inlets.

The purpose of the center tube is to transmit all the aerodynamic drag from the Ballute to the canister. The base drag is transferred to the center tube by means of the aft attachment, while the front or impact drag is transmitted through the forward attachment. The total load is then transferred to the canister by means of the canister attachment. The center tube design incorporates chafing strips at the forward and aft attachments to prevent damage to the Ballute during the inflation process. The center tube is constructed from the same type of material that is used in the basic Ballute.

The Ballute is the drag producing body. It is constructed from four forward and four aft gores which have been heat-formed to the prescribed shape. Shape form is achieved by affixing Griege goods to a mold and then applying heat at 325°F for 15 minutes. Griege goods are fabrics that have not been heat set as part of its normal manufacturing processes. Fabrics woven from thermal sensitive synthetic yarns, such as nylon, are heat treated and tensioned

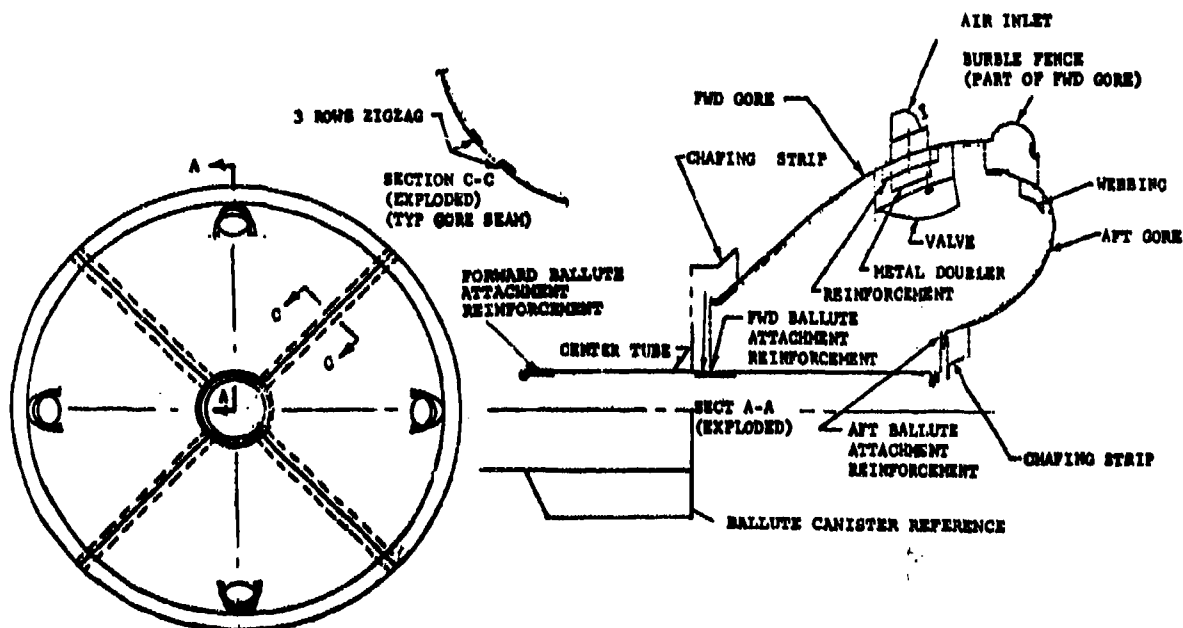


Figure 7. MK82 Ballute Descriptive Details

during manufacturing to improve the strength-to-weight and rupture elongation characteristics. The Ballute is assembled by sewing the gores together with a zig-zag stitch. The material used in the Ballute is square-woven Nylon². ("Square woven" indicates that the strength is the same in both the fill and the warp directions.) Fabrics utilized in this effort are woven with two sets of yarns oriented perpendicular to each other. The set of yarns that is oriented in the direction of the fabric as it unrolls is known as warp yarn, and the direction is referred to as the warp direction. The remaining set of yarns are oriented in the direction across the roll of fabric and is known as fill yarn. This direction is referred to as the fill direction. Normally, the warp direction is synonymous with the length and the fill direction is synonymous with the width of the fabric. The Ballute for the mine device is 29 inches in diameter (referred to as 29-inch Ballute) and is constructed using fabric rated at 1050 pounds per inch in both directions (warp and fill). The Ballute for the GP bomb is 41 inches in diameter (referred to as a 41-inch Ballute) and is constructed using fabric rated at 1500 pounds per inch in both directions.

It should also be noted that the fabric for the 41-inch Ballute is uncoated. Some of the advantages of using uncoated over coated fabrics are:

- (1) Better structural integrity since individual yarns in uncoated fabric can orient themselves to the direction of the applied load.
- (2) Higher strength-to-weight ratio since coating is not added.
- (3) Easier packaging since coated fabric tends to be stiff and rigid.

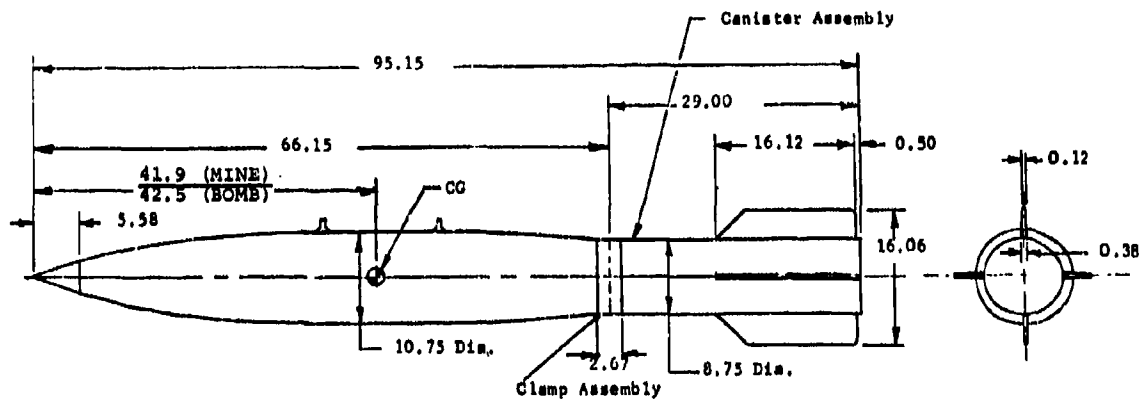
Subsequent to the fabrication of the 29-inch Ballutes, analysis of in-house tests indicated that the porosity of the fabric was at least two times greater than the 41-inch Ballute fabric. Accordingly, the fabric for the 29-inch Ballutes was coated with a PRC (synthetic rubber) compound to reduce fabric porosity to insure proper low launch speed inflation.

The burble fence is an aerodynamic device that is attached aft of the Ballute's equator. Its purpose is to uniformly trip the airflow over the aft portion of the Ballute, which provides a stabilizing effect at subsonic speeds. The burble fence uses the same construction techniques and the same type of fabric as the Ballute.

The inlets used are semi-circular in shape and fabricated from corrosion-resistant steel. The 29-inch Ballute is provided with eight inlets; the frontal area of each inlet is 1.03 square inches for a total of 8.24 square inches per Ballute. The 41-inch Ballute has four inlets; the frontal area of each inlet is 5.97 square inches for a total of 23.88 square inches.

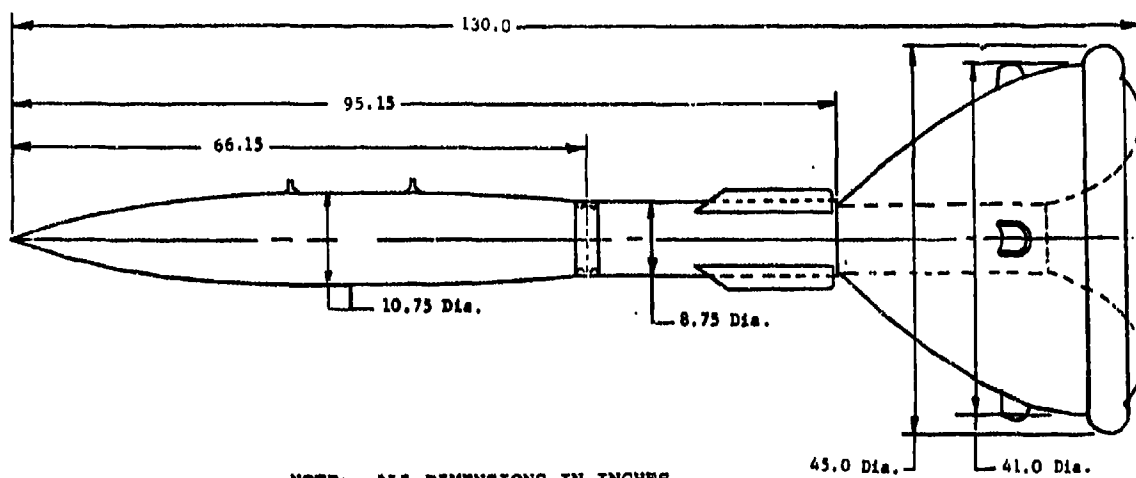
Basic dimensions for the three configurations are presented in Figures 8, 9, and 10.

²T.M., E. I. DuPont de Nemours & Co., Inc., Wilmington, Del.



NOTE: ALL DIMENSIONS IN INCHES

Figure 8. MK82 Low-Drag Configuration



NOTE: ALL DIMENSIONS IN INCHES

Figure 9. MK82 GP Bomb High-Drag Configuration

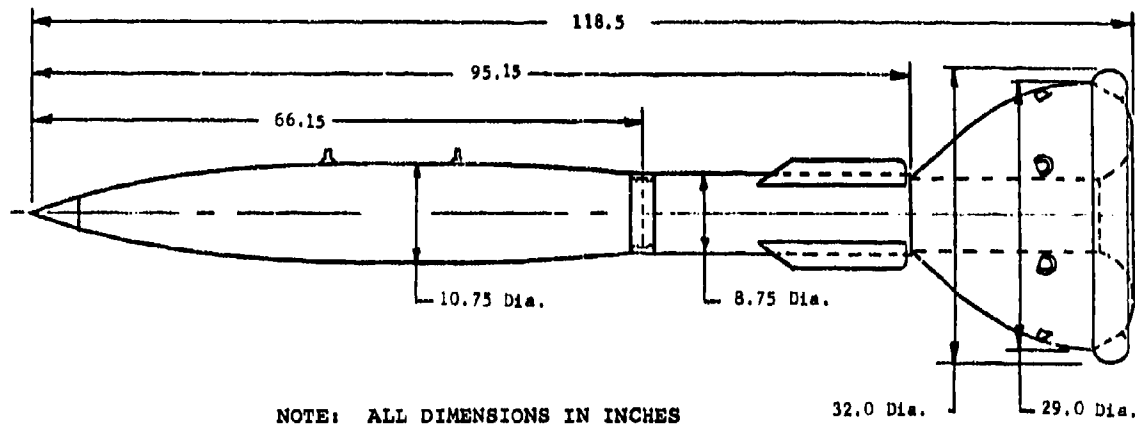


Figure 10. MK82 Mine Device High-Drag Configuration

SECTION IV
AERODYNAMIC ANALYSES

1. STABILITY OF THE MK82 BOMB WITH A BALLUTE CANISTER

The MK82 bomb modified with a Ballute canister afterbody was analyzed in order to determine the tail panel (fin) size required to provide a static margin at subsonic speeds equal to that of the original MK82 bomb. The static stability margin of the MK82 Ballute/canister was estimated by combining the body-alone aerodynamic characteristics with estimated contributions for the tail panel and the tail-body interference. For the analyses, a tail panel leading edge sweep of 45° was considered and tail panel chord length was varied. Body-alone wind-tunnel data from Reference 1 and the tail panel aerodynamic characteristics as determined by the methods of Reference 2 were used. Good agreement with the tail panel plus tail-body interference characteristics of the one caliber tail panel of Reference 1 was achieved with this procedure.

Stability margins were estimated for MK82/Ballute canister combinations employing tail panels with a 16-inch span and various root chord lengths mounted on both a 26-inch and a 29-inch long canister. To show the effect of varying the tail panel span, the stability margins for a 15-inch span and a 17-inch span, one caliber root chord tail panel also was estimated. The results of this analysis, presented in Figure 11, show that all cases examined yielded subsonic speed static margins in excess of 1.3 caliber. Additional static margin can be achieved by increasing the span.

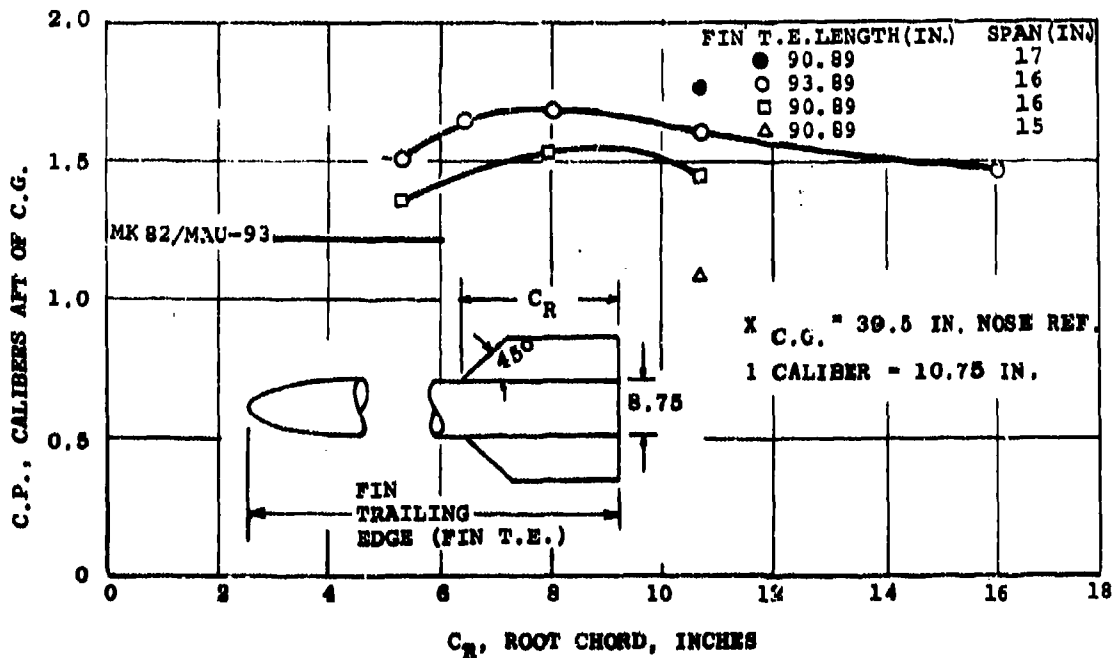


Figure 11. Estimated Variation of Center of Pressure at Low Subsonic Velocities - MK82/Ballute Canister

As a result of the analysis, a 3/4 caliber (8.05-inch chord) tail panel with a 16-inch span was recommended for use on the modified MK82 bomb with a Ballute canister afterbody. The stability of the modified bomb should be comparable to that of the original MK82.

It should be noted that chronologically the above recommendation was made prior to the analysis of AFATL wind tunnel tests on MK82/Ballute canister configurations with 3/4, 1, and 1-1/2 caliber (root chord) fins. Also, prior to the analysis, the contractor had to release procurement instructions for canister castings. These procurement instructions were released for the 1-1/2 caliber fin configuration because it would be easier to shorten than to lengthen the cast aluminum fins. Subsequently, the analysis of wind tunnel test data did not indicate any trend of fin stability. Accordingly, it was decided, with AFATL agreement, to initiate flight testing with the longer 1-1/2 caliber fin since shortening of the fin, if required, would necessitate a minimal effort.

2. DESIGN LOADS FOR THE 3/4 CALIBER TAIL PANEL AND FOR THE 1-1/2 CALIBER TAIL PANEL

The aerodynamic forces on the 3/4 caliber tail panel and on the 1-1/2 caliber tail panel were calibrated for the two cases noted below. Case 1 tail loads were used to determine the structural design of the tail, while Case 2 tail panel loads were used along with the Ballute loads of subsection 5 to determine the clamp assembly structural requirements.

| <u>Case</u> | <u>Description</u> | <u>Mach No.</u> | <u>Altitude (feet)</u> | <u>Angle of Attack (degrees)</u> | <u>Dynamic Pressure (psf)</u> |
|-------------|------------------------------------|-----------------|------------------------|----------------------------------|-------------------------------|
| 1 | Tail Fin Structural Analysis | 1.30 | 10,000 | ±20 | 1721 |
| 2 | Clamp Assembly Structural Analysis | 0.91 | 250 | ±20 | 1230 |

The analyses of the tail panel airloads were based on the methods of References 2 and 3 and considered both the loads on the tail panel in the presence of the body and the carryover loads from the tail panel onto the canister body. The nonlinear forces at angle of attack due to viscous cross flow were analyzed based on results for similar configurations, Reference 4. The normal forces and centers of pressure for the two tail panels are shown for the two design cases. It should be noted that the centers of pressure are measured from the trailing edge of the tail panel and that the tail panel load refers to the normal force on a single tail panel.

DESIGN LOADS FOR THE 3/4-CALIBER TAIL PANEL (FIN)

| Case | Fin Normal Force (lb) | Fin Center of Pressure (in.) | Fin + Carryover Normal Force (lb) | Fin + Carryover Center of Pressure (in.) |
|------|--------------------------|---------------------------------|--------------------------------------|---|
| 1 | 420 | 4.03 | 1050 | 3.50 |
| 2 | 290 | 5.16 | 810 | 5.38 |

DESIGN LOADS FOR THE 1-1/2-CALIBER TAIL PANEL (FIN)

| Case | Fin Normal Force (lb) | Fin Center of Pressure (in.) | Fin + Carryover Normal Force (lb) | Fin + Carryover Center of Pressure (in.) |
|------|--------------------------|---------------------------------|--------------------------------------|---|
| 1 | 475 | 11.0 | 1310 | 9.2 |
| 2 | 334 | 12.8 | 896 | 13.2 |

The Ballute load calculated as a part of the Case 2 clamp assembly structural analysis is discussed in subsection 5.

3. BALLUTE PRESSURE DISTRIBUTION

A pressure distribution over the fully inflated 41-inch Ballute was developed for use in the structural analysis of the Ballute. The design condition selected was 1212 feet/second at 2000 feet altitude, corresponding to a design Mach number of 1.1. The pressure distributions were derived using the experimental data of Reference 5. The resulting pressure distributions are plotted in Figure 12. The original pressure distribution estimate shown in the figure was made during the program's proposal stage and has since been revised in accordance with a more detailed analysis of the experimental data. Both pressure distributions, when integrated, yielded drag coefficients larger by 10 to 20 percent than would be predicted based on the analysis of the following section.

Therefore, the results of the structural analysis are conservative, and the Ballute should be capable of sustaining loads in excess of those actually associated with the design condition. These larger drag values resulting from the integrated pressure distribution may be explained by the presence of separated flow regions on the Ballute surface which are not taken into account in the estimated pressure distributions.

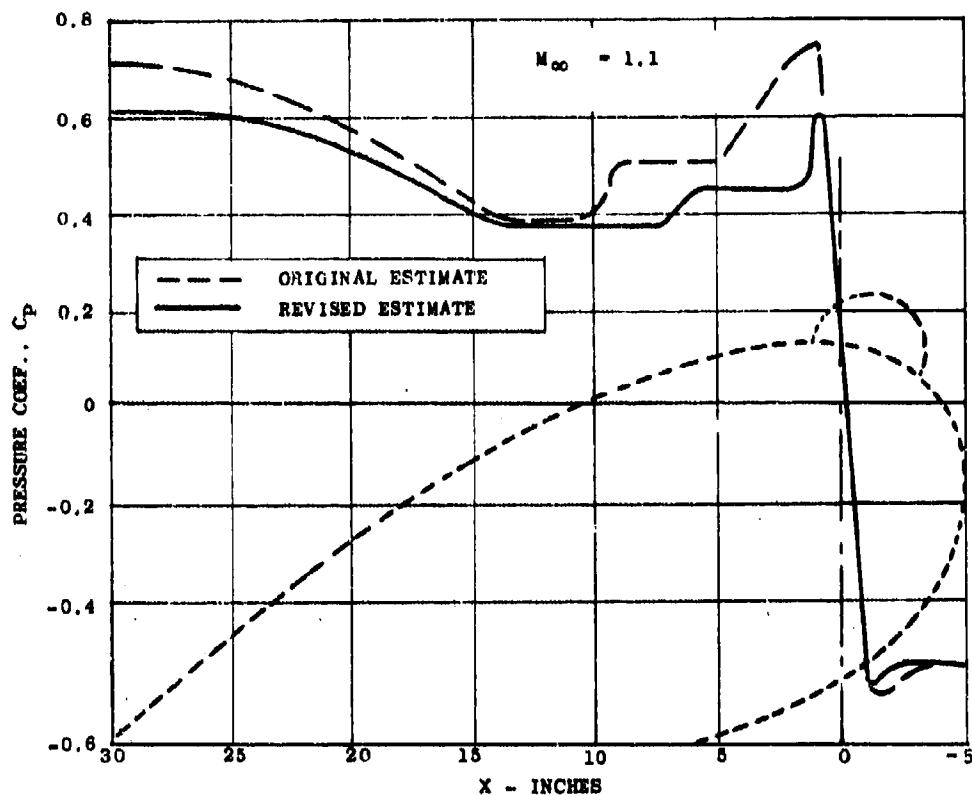


Figure 12. Estimated Pressure Distribution - 41-Inch Ballute

4. BALLUTE DRAG COEFFICIENT

The incremental zero-lift drag coefficient for the Ballute in the presence of the MK82 bomb forebody were estimated based on the M-117 Ballute results of Reference 6. The incremental drag coefficients were determined for both the 29-inch and the 41-inch Ballutes, and the results, referenced to the bomb cross-sectional area, are presented in Figure 13. To determine the total drag coefficient for the MK82/inflated Ballute, the bomb-alone drag coefficient (although small compared to that of the Ballute) should be added to the drag values of Figure 13.

5. DESIGN LOADS FOR 41-INCH BALLUTE AND CANISTER

The aerodynamic forces on the 41-inch Ballute were calculated for the design cases listed below:

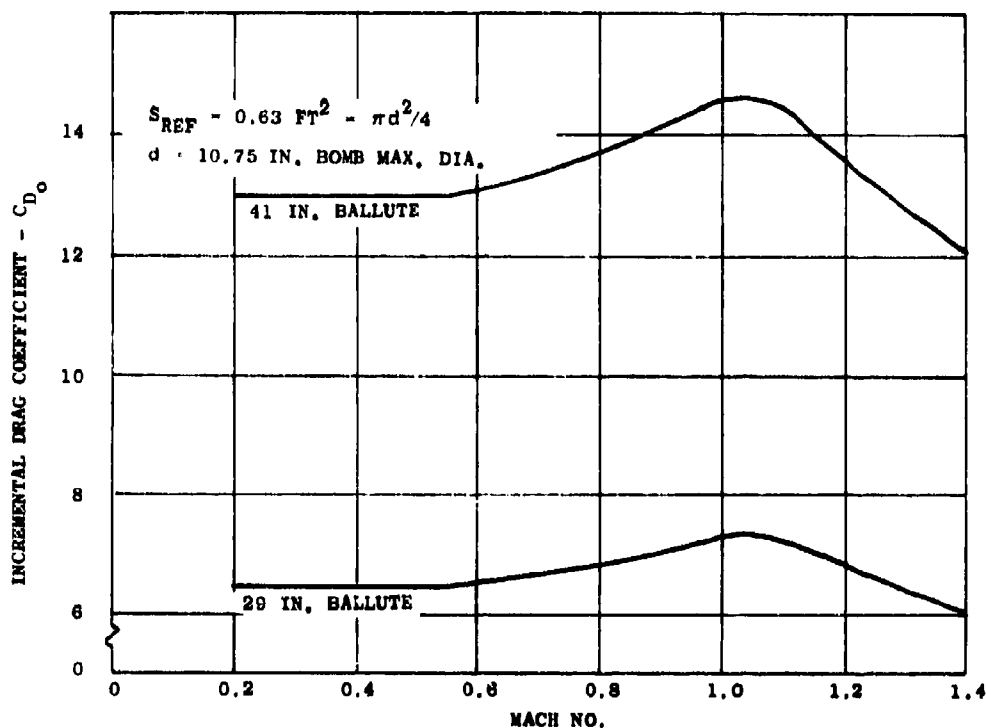


Figure 13. Estimated Variation of Ballute Incremental Drag

| <u>Case</u> | <u>Description</u> | <u>Mach No.</u> | <u>Altitude (feet)</u> | <u>Angle of Attack (degrees)</u> | <u>Dynamic Pressure (psf)</u> |
|-------------|------------------------------------|-----------------|------------------------|----------------------------------|-------------------------------|
| 2 | Clamp Assembly Structural Analysis | 0.91 | 250 | ± 20 | 1230 |
| 3 | Ballute Structural Analysis | 1.1 | 2000 | 0 | 1650 |

Case 2 defines the clamp assembly design condition and includes the aerodynamic loads transmitted to the canister from both the Ballute and the 3/4 caliber tail (see tail analysis of subsection 2). For the Case 2 analysis, the Ballute was assumed rigid and undeformed at 20° angle of attack. The Ballute aerodynamic wind tunnel data of Reference 7 shows that the Ballute drag coefficient is almost constant with angle of attack and that the Ballute lift coefficient is approximately zero for all angles of attack. Then, for 20° angle of attack at Mach 0.91, the Ballute drag coefficient (C_D), lift coefficient (C_L), based on the forebody reference area ($S_{REF} = 0.63 \text{ ft}^2$), are

$$C_D = 14.1 \quad C_L = 0$$

Transforming the above wind-axis coefficients into the body-axis system and multiplying by the dynamic pressure of 1650 psf and the reference area 0.63 ft², the forces on the Ballute are as follows:

Normal Force = 3420 lb
 Axial Force = 10,250 lb

From the analysis of the data of Reference 8, the Ballute center of pressure was estimated to be 5.4 inches aft of the Ballute base.

For the Case 3, 41-inch Ballute structural analysis, the Mach 1.1 drag load, calculated from Figure 13, is 15,000 pounds.

6. MK82 BOMB/BALLUTE TERMINAL VELOCITIES

For a system weight of 550 pounds, the steady-state terminal velocities were computed for the MK82 with the fully inflated 29-inch Ballute and 41-inch Ballute. The drag coefficients for these systems, as well as for the MK82/Ballute canister, are shown in Figure 14. The drag of the MK82/Ballute

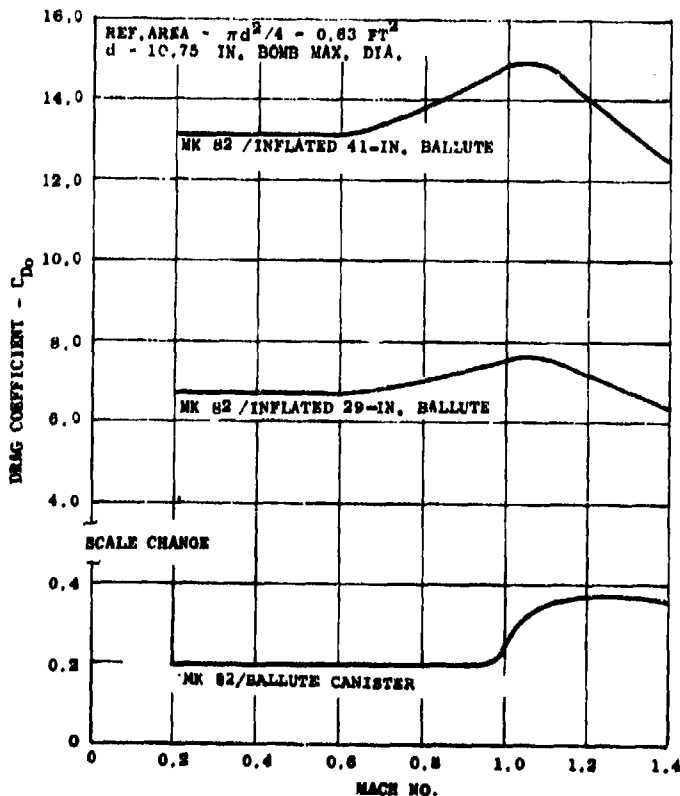


Figure 14. Estimated Variation of Drag Coefficients

canister was estimated by determining the incremental drag due to the change in afterbody shape from a boattail to a cylinder and adding this to the basic MK82 wind tunnel drag data of Reference 9. The MK82/inflated Ballute drag is the total of the MK82 drag and the incremental Ballute drag from Figure 13.

Terminal velocity, V_T was calculated from the equation

$$V_T = \left[\frac{2}{\rho} \times \frac{W}{C_D S_{Ref}} \right]^{1/2}$$

where ρ = Sea level density = 0.002378 slug/ft³

W = Weight = 550 lb

C_D = Drag coefficient

S_{Ref} = Reference area = 0.63 ft²

Results of these calculations are

V_T = 338 ft/sec (MK82/29-inch Ballute)

V_T = 241 ft/sec (MK82/41-inch Ballute)

The 241 ft/sec terminal velocity with the 41-inch Ballute satisfies closely the design goal, while the 338-ft/sec terminal velocity with the 29-inch Ballute system undershoots the design goal of a 400-ft/sec impact velocity. It should be noted that the computed terminal velocities are the minimum velocities at which impact will occur. The utilization of the 29-inch system is based on pre-contract analysis conducted by the contractor. A result of this analysis indicated that a 29-inch Ballute will satisfy the impact velocity design goal of 300 to 400 feet per second.

7. EFFECT OF MACH NUMBER ON STABILITY

The static stability characteristics for the MK82/Ballute canister were analyzed by considering the stability contributions of the bomb plus Ballute canister separately from that of the tail panels. For the Ballute canister without tail panels, the MK82 bomb alone (no tail) wind tunnel data from References 1 and 10 were adjusted to account for the presence of the cylindrical Ballute canister in place of the boattail section on the original MK82. Adjustments were derived from a comparison of bomb (without tail) data with stability data on a 2.5-caliber ogive plus cylindrical afterbody from Reference 11.

The effect of these adjustments to $C_{m\alpha}$ and $C_{N\alpha}$ was to increase the stability of the MK82/Ballute canister over that of the MK82 bomb body alone due to elimination of the destabilizing boattail. The resulting MK82 Ballute canister without tail panels $C_{N\alpha}$ and $C_{m\alpha}$ are shown as a function of Mach number in Figures 15 and 16, respectively.

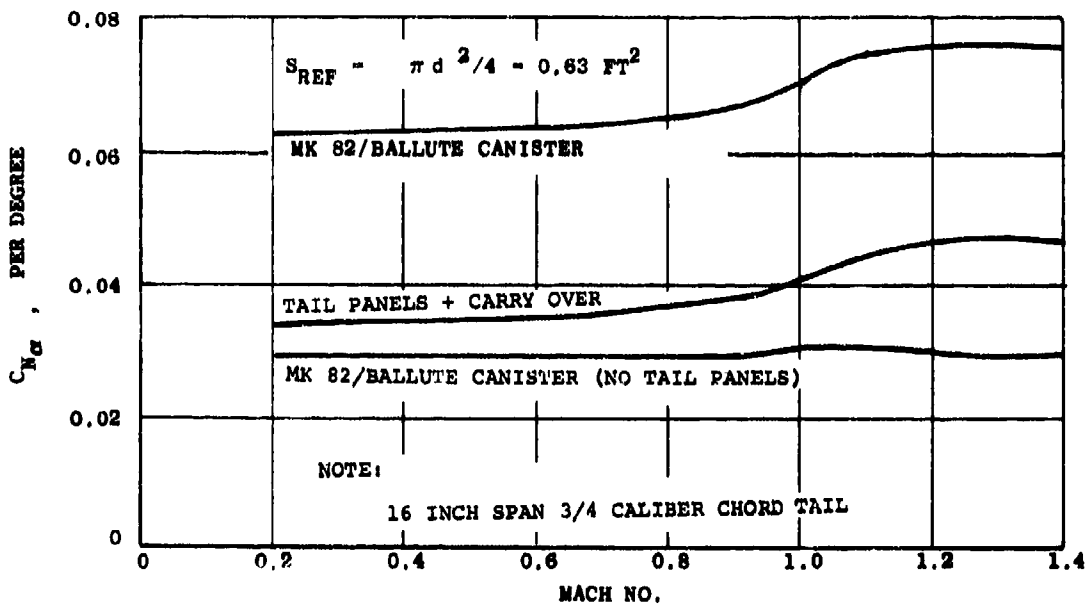


Figure 15. Estimated Variation of Normal Force Coefficient

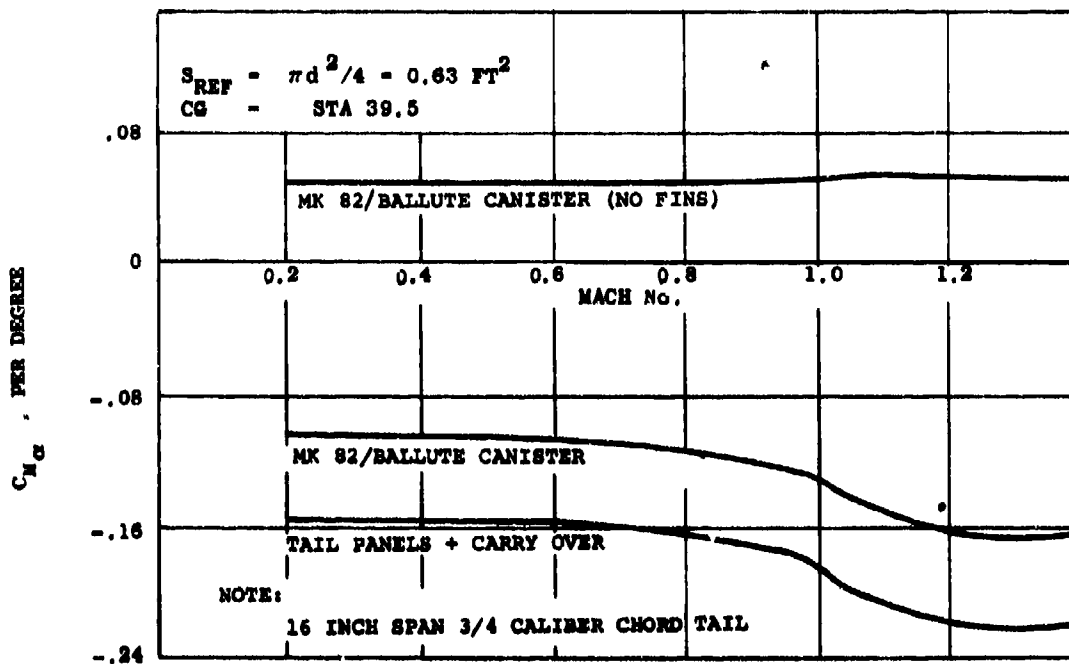


Figure 16. Estimated Variation of Pitching Moment Coefficient

The stability contribution of the 3/4-caliber cruciform tail panels was determined as in References 2 and 12 based on linear aerodynamic characteristics at small angles of attack. The resulting $C_{N\alpha}$ and $C_{m\alpha}$ due to the tail lift in the presence of the canister and the lift carryover from the tail onto the canister are shown in Figures 15 and 16, along with the total $C_{N\alpha}$ and $C_{m\alpha}$ for the MK82/Ballute canister. The static margin (s.m.) is defined as follows:

$$\text{s.m.} = C_{m\alpha} / C_{N\alpha}$$

It is measured in calibers forward from the MK82 center of gravity (Reference Station 39.5) and is plotted in Figure 17 as a function of Mach number. (Note that a stable vehicle will have a negative static margin.)

For comparison, the static margin of the original MK82/MAU-93 is also plotted on Figure 17. At all Mach numbers, the stability of the MK82/Ballute canister with a 3/4-caliber tail exceeds that of the original MK82 bomb.

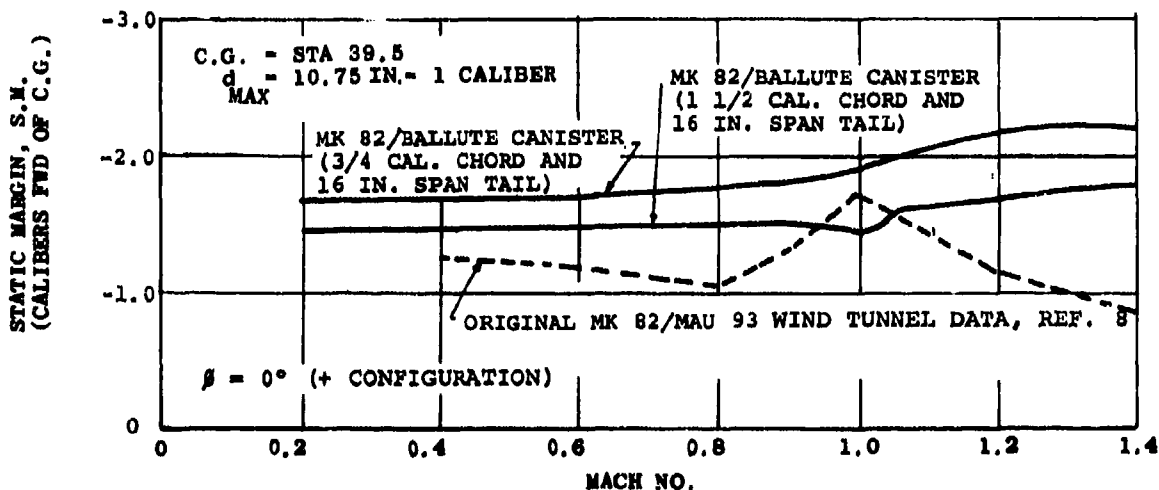


Figure 17. Estimated Variation of Static Margin with Mach Number

The above stability analysis was repeated for the 1-1/2-caliber tail panels, and the resulting static margins are shown in Figure 17. For most Mach numbers, the stability of the MK82/Ballute canister with 1-1/2-caliber tail panels exceeds that of the original MK82 bomb.

8. EFFECT OF ROLL ATTITUDE ON STATIC STABILITY

The preceding stability analyses were performed with the MK82/Ballute canister at zero roll angle ($\phi = 0$). This corresponds to a plus configuration in which the angle-of-attack vector lies in the plane of one pair of opposing tail panels. Stability characteristics determined at $\phi = 0$ generally are assumed valid (with only small error) at other roll attitudes, and this assumption normally would be used herein. However, at least for the original MK82, several questions have arisen regarding the variation of static margin with roll attitude.

To investigate these questions, a review was made of the wind tunnel data of References 1 and 9 for the original MK82 and Reference 10 for the MK82 with a Naval Ordnance Laboratory (NOL) modified tail (larger fin; 15 percent greater area). In Figure 18, the original MK82 bomb static margin is plotted versus Mach number for both $\phi = 0^\circ$ and $\phi = 45^\circ$ roll attitudes. An unusually large variation of static margin with roll attitude is observed in the vicinity of Mach 1.0. For the MK82/NOL tail, the static margins plotted in Figure 19 show a significant dependence on roll attitude at all Mach numbers with the difference in static margin maximized at Mach 1.0. While the values of static margin for the original MK82 at $\phi = 0$ increase greatly near Mach 1.0, the static margin at $\phi = 0$ for the modified tail MK82 decreases near Mach 1.0. To further confuse the situation, the wind tunnel data of Reference 13 for the M-117 bomb (which is similar to the MK82) is plotted in Figure 20 and shows almost no effect of roll attitude on static margin, even near Mach 1.0.

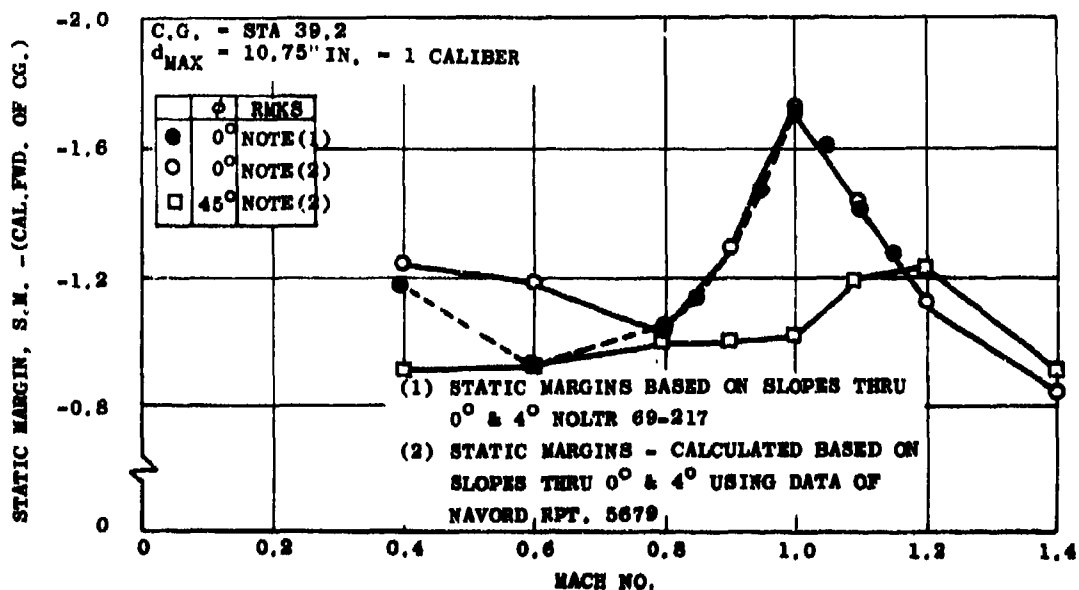


Figure 18. Variation of Static Margin with Mach Number and Roll Attitude - MK82/HAU-93

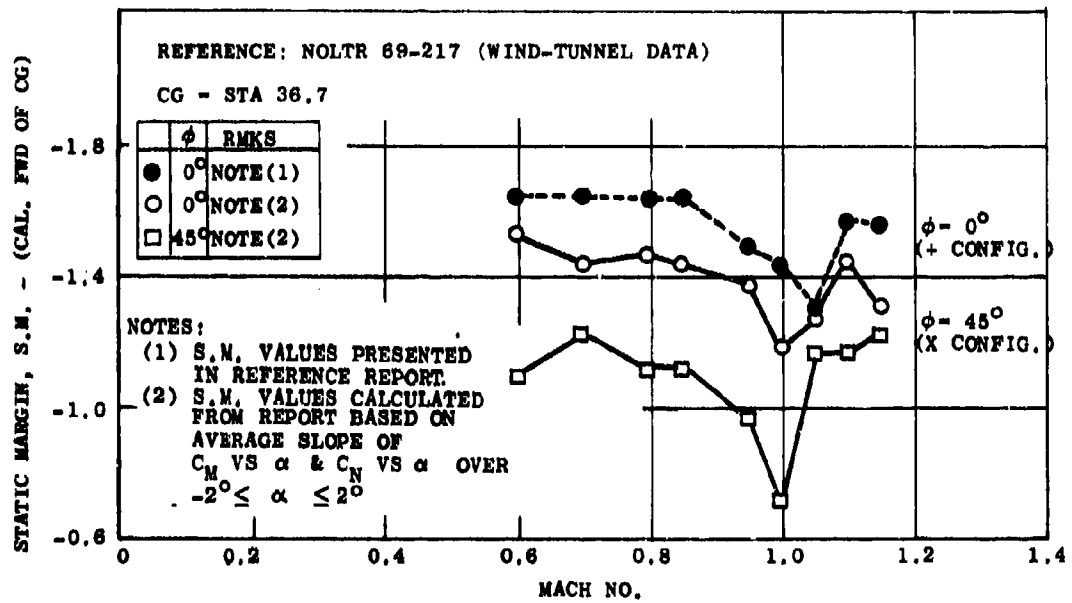


Figure 19. Variation of Static Margin with Mach Number and Roll Attitude - MK82/NOL Tail

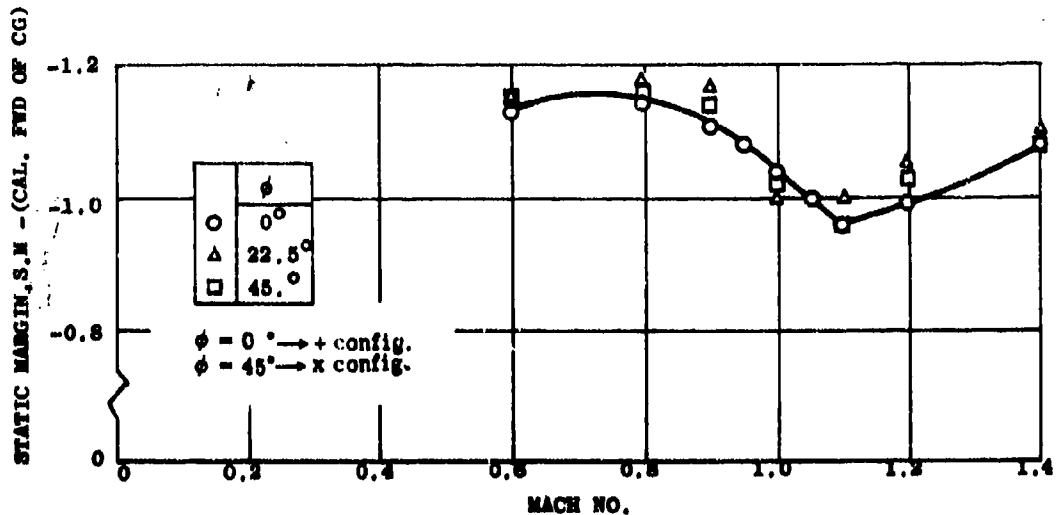


Figure 20. Variation of Static Margin with Mach Number and Roll Attitude - M-117 Bomb

The differences in geometries of the cited configurations do not offer any clue to the flow mechanism causing the measured variations in stability with roll attitude, although any variation would presumably be related to the change in downwash and crossflow fields impinging on the tail panels.

The effect of roll angle on stability that will result by replacing the MAU-93 tail with the Ballute canister is not known. Only by performing a static stability wind tunnel test of the MK82/Ballute canister munition can this effect be determined.

9. DYNAMIC STABILITY CONSIDERATIONS

For the original MK82/MAU-93, flight instabilities have occurred in some of the bomb drops. These instabilities occur at transonic speeds and produce a coning motion similar to a pitch-roll coupling. This MK82 dynamic instability may be caused, in part, by the large variation of static margin with roll attitude, as shown in Figure 18. However, no dynamic analysis of this system has been performed, and any statement as to cause would be speculative.

For the MK82/NOL modified tail, no flight instabilities have been observed in the 36 flights to date. However, this small number of flights precludes the conclusion that the problem is solved. Also, from Figure 19, the MK82/NOL modified tail has a large variation of static stability with roll attitude and only a slight increase in the levels of static margin over the original MK82/MAU-93 (taking into account the different moment reference centers in Figures 18 and 19).

Since the cause of the observed flight instability is unknown, it is not possible to design the MK82/Ballute canister so as to avoid the cause of the flight instability. The munition can be designed with the highest possible level of static stability consistent with the imposed length and span constraints. It would, of course, be desirable to design the vehicle so as to minimize the variation of static margin with roll attitude. Neither of these steps will ensure a dynamically stable munition.

There is one additional consideration insofar as achieving a dynamically stable munition is concerned. The munition should be designed to minimize the possibility of pitch-roll resonance. To do this, many munitions, including the MK82, have used canted tail surfaces to produce a sufficiently high acceleration and steady-state spin rate so as to drive through and remain above the munitions' natural pitching frequency and thus avoid pitch-roll instability. The MK82/Ballute canister does not currently employ any aerodynamics spin system. While tail cant may be unnecessary, especially during the first phase of the program, the possibility of using canted tail panels at a later date should be kept in mind.

10. CONCLUSIONS AND RECOMMENDATIONS

From the analyses, the following are concluded:

- (1) The static margin of the MK82/Ballute canister with 3/4-caliber tail chord exceeds that of the original MK82/MAU-93 at all Mach numbers of interest.

- (2) The variation with roll attitude of static margin cannot be predicted either analytically or by comparison with existing wind tunnel data.
- (3) The dynamic stability of the MK82/Ballute canister cannot be predicted. The magnitude of the static margin, the effect of roll attitude on static stability, and the proper fin cant can contribute to reducing the likelihood of a dynamic instability occurring.

To obtain information to ensure a stable vehicle, a wind tunnel test program is recommended. This program will supply aerodynamic data not presently available. The test matrix should include Mach numbers from 0.2 to 1.4 and angle of attack from -5° to $+30^{\circ}$. The tests will be directed toward obtaining the following information on the MK82/Ballute canister:

- (1) Effect of roll attitude on static stability

Six component force and moment data should be measured at $\phi = 0^{\circ}$, 22.5° , and 45° .

- (2) Accurate linear and nonlinear static aerodynamic characteristics

In conjunction with item 1, data will be obtained to verify the predicted linear characteristics and to ensure static stability at high angles of attack.

- (3) Dynamic stability characteristics

Tests should be performed to define the dynamic stability of the munition at various Mach numbers and angles of attack.

- (4) Effect of tail planform on static and dynamic stability

Planform variations (leading edge sweep, chord length, etc.) should be considered to determine the optimum statically and dynamically stable configurations.

- (5) Effect of tail cant on static and dynamic stability

The effect on aerodynamic characteristics of varying tail cant angle should be determined.

In addition to the wind tunnel test program, the test results should be employed in performing six-degree-of-freedom computer simulations to analyze munition flight stability.

SECTION V
STRUCTURAL ANALYSIS

1. GENERAL

The objective of this section is to show the ability of the Ballute retarder system to withstand the loads imposed during flight as discussed in Section IV, Aerodynamic Analysis. This section is presented in two parts, namely fabric analysis and metal analysis.

2. FABRIC ANALYSIS

a. Dynamic Stresses During Ballute Deployment

Ballute deployment is initiated by release of the aft-cover plate (Item 8 of Figure 2). The differential base pressure acts on this plate to provide the extraction force that extends the uninflated Ballute parallel to the bomb's longitudinal axis of revolution. Full extension corresponds to the fabricated length of the inner fabric sleeve as shown in Figure 21.

The base drag pressure coefficient is taken from Figure 12 as,

$$C_{p_b} = -0.53 \quad (\text{Also plotted in Figure 28}).$$

The governing loading condition is Case 3, page 17 for which the dynamic pressure is,

$$q = 1650 \text{ pounds per square foot}$$

or,

$$q = \frac{1650}{144} = 11.45 \text{ pounds per square inch.}$$

Hence, by definition,

$$p_b = C_{p_b} q = -(0.53) (11.45) = -6.068 \text{ pounds per square inch}$$

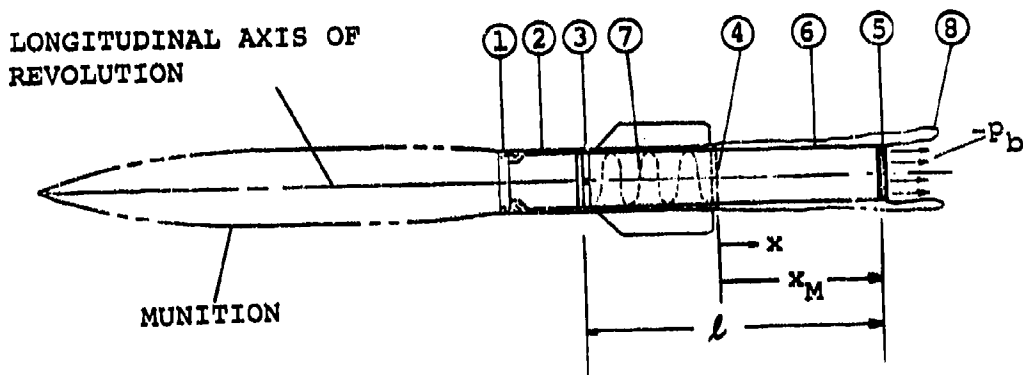
The diameters of the inner fabric sleeve and of the cover plate are considered equal to the inner diameter from Figure 5; i.e.,

$$d_1 = 8.0 \text{ inches.}$$

The extraction force is,

$$F_e = -p_b \frac{\pi}{4} d_1^2 = (6.068) \left(\frac{\pi}{4} \right) (8)^2 = 305 \text{ pounds.}$$

This force is essentially constant during extraction so that the total work done is simply,



- (1) CLAMP ASSEMBLY
 - (2) CANISTER ASSEMBLY
 - (3) FORWARD BALLUTE ATTACHMENT
 - (4) AFT BALLUTE ATTACHMENT AND COVER PLATE PRIOR TO DEPLOYMENT
 - (5) AFT BALLUTE ATTACHMENT AND COVER PLATE AT FULL EXTENSION
 - (6) INNER FABRIC SLEEVE
 - (7) PACKAGED BALLUTE
 - (8) UNINFLATED BALLUTE AT FULL EXTENSION
- l - FABRICATED LENGTH OF THE INNER FABRIC SLEEVE - 42 INCHES FOR THE 41-INCH DIAMETER BALLUTE AND 35 INCHES FOR THE 29-INCH DIAMETER BALLUTE
 x - LONGITUDINAL DISPLACEMENT OF THE COVER PLATE, IN INCHES
 x_M - MAXIMUM LONGITUDINAL DISPLACEMENT OF THE COVER PLATE - 24 INCHES FOR THE 41-INCH DIAMETER BALLUTE AND 17 INCHES FOR THE 29-INCH DIAMETER BALLUTE
 P_b - DIFFERENTIAL BASE PRESSURE IN POUNDS PER SQUARE INCH

Figure 21. Longitudinal Extraction of the Uninflated Ballute

$$W_e = x_M F_e = (24)(305) = 7320 \text{ inch-pounds.}$$

This work must be absorbed as strain energy in the inner fabric sleeve. The unit strain energy to be absorbed is,

$$u = \frac{W_e}{\pi l d_1} = \frac{7320}{\pi(42)(8)} = 6.935 \text{ inch-pounds per square inch.}$$

The sleeve is constructed of a single ply of fabric having the warp and fill threads oriented in the longitudinal and circumferential directions, respectively. Therefore, only the longitudinal threads absorb the above energy.

A typical stress-strain curve for high tenacity, nylon filament yarns, as taken from Reference 14, is plotted in Figure 22. As shown, the breaking tenacity is 7.5 grams per denier. The ultimate breaking strength of the sleeve fabric for the 41-inch diameter Ballute is,

$$F_{tu} = 1500 \text{ pounds per inch in the warp direction,}$$

$$F_{tu} = 1500 \text{ pounds per inch in the fill direction.}$$

On this basis, the ordinate scale of stress in pounds per inch is added to Figure 22. Setting the area under the stress-strain curve equal to the required unit strain energy gives the desired longitudinal stress level,

$$\frac{\sigma^2}{2E} = u,$$

$$\sigma = \sqrt{2Eu} = \sqrt{2(4100)(6.935)} = 238 \text{ pounds per inch.}$$

For an ultimate factor of safety of F.S. = 2, the margin of safety is,

$$M.S. = \frac{F_{tu}}{(F.S.)(\sigma)} - 1 = \frac{1500}{(2)(238)} - 1 = \underline{+2.15} \text{ for the}$$

41-inch diameter Ballute).

The 29-inch diameter Ballute will also be deployed at $q = 1650$ pounds per square foot (Case 3). The preceding equations are applied in the following calculations to determine the margin of safety for the inner fabric sleeve:

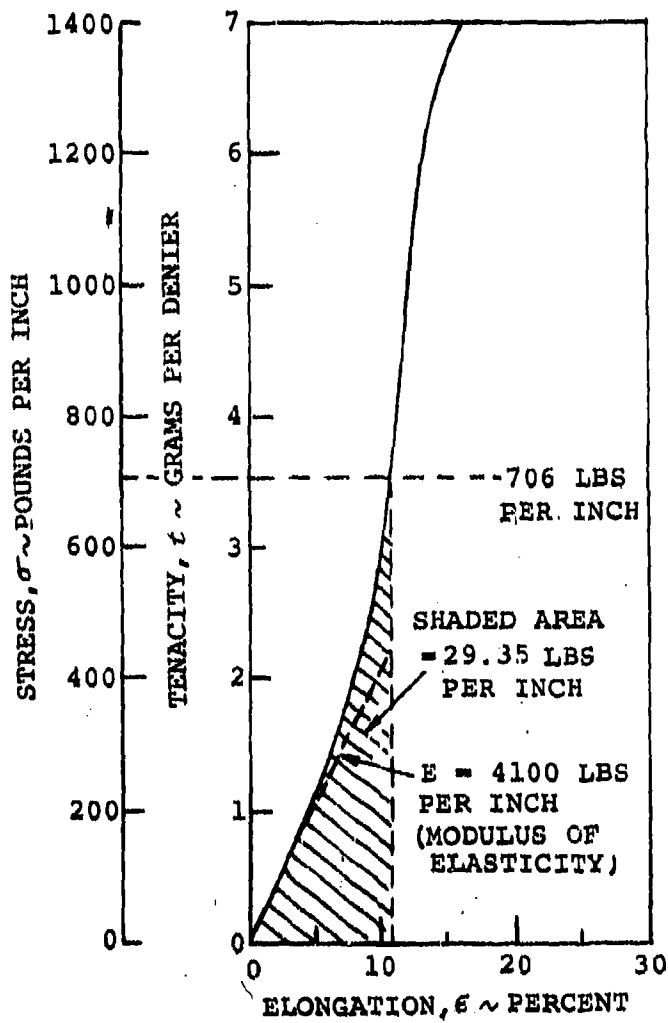


Figure 22. Typical Stress-Strain Curve for High Tenacity Nylon Filament Yarns

$$W_e = x_M F_e = (17)(305) = 5185 \text{ inch-pounds,}$$

$$u = \frac{W_e}{\pi l d_i} = \frac{5185}{\pi (35)(8)} = 5.895 \text{ inch-pounds per square inch}$$

The sleeve is constructed identically to that of the 41-inch diameter Ballute except that the ultimate breaking strength is,

$$F_{tu} = 1050 \text{ pounds per inch in the warp direction}$$

$$F_{tu} = 1050 \text{ pounds per inch in the fill direction}$$

Therefore,

$$E \approx \left(\frac{1050}{1500} \right) (4100) = 2870 \text{ pounds per inch}$$

$$\sigma = \sqrt{2Eu} = \sqrt{2(2870)(5.895)} = 184 \text{ pounds per inch}$$

$$\text{M.S.} = \frac{F_{tu}}{(F.S.)(\sigma)} - 1 = \frac{1050}{(2)(184)} - 1 = +1.85 \text{ (for the 29-inch diameter Ballute).}$$

Subsequent to the longitudinal extraction of the uninflated Ballute as shown in Figure 21, the ram-air inlets (see Figure 2) are exposed to the air stream. The influx of air causes the Ballute to grow in the radial direction from the initial shape of Figure 21 to the fully inflated shape of Figure 2. Any given cross section of the Ballute, taken normal to the axis of symmetry, will expand during inflation until it reaches its maximum diameter. At this instant, a circumferential dynamic stress occurs because the radial velocity component of the internal air mass must be stagnated.

It is possible to calculate this circumferential stress by equating the strain energy-absorbing capacity of the Ballute fabric to the kinetic energy of the internal air since this energy must be absorbed by the fabric at the instant of full inflation.

The largest circumferential stress occurs on the cross section of unit width that travels the largest radial distance. This hoop of fabric is located at the equator of the Ballute as shown in Figure 23. The kinetic energy of the inflation air pushing upon this hoop can be found by writing an expression for the pressure force applied to a differential element at any radius, r , then integrating over all values of r and over a radial angle of 2π .

$$JW = prd\theta dr \quad (\text{refer to Figure 24})$$

$$W = \int_{r_b}^R \int_0^{2\pi} prd\theta dr = 2\pi \int_{r_b}^R prdr \quad (1)$$

where, (refer to Figure 24)

- W = the applied kinetic energy in inch-pounds
- p = the internal air pressure in pounds per square inch
- r_b = the initial radius of the expanding unit width hoop in inches
- R = the final radius of the expanding unit width hoop in inches.

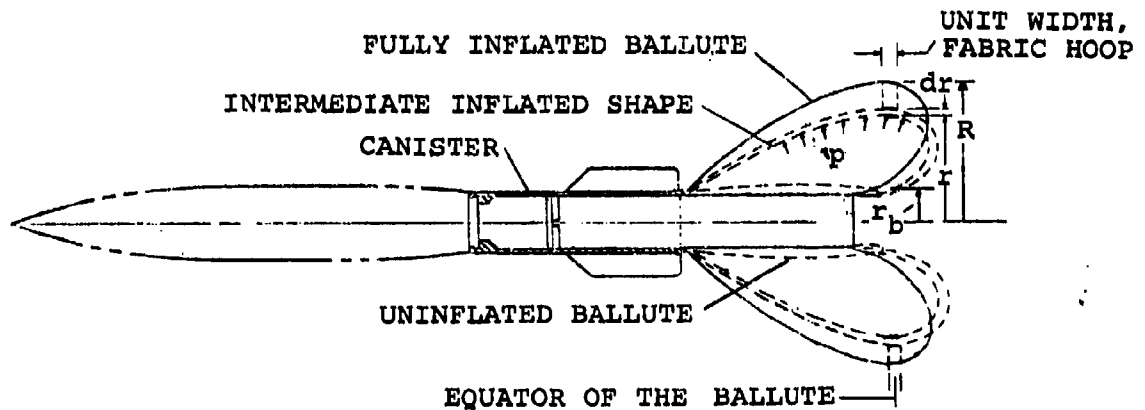


Figure 23. Radial Expansion of the Inflating Ballute

In order to integrate equation (1), the internal pressure must be expressed as a function of the radius. Estimation of this function is based upon the following logic:

- (1) Upon exposure of the ram-air inlets to the air stream, the Ballute does not expand until the internal air pressure becomes greater than the external air pressure. Hence, at $r = r_b$, the differential pressure is, $p = 0$.

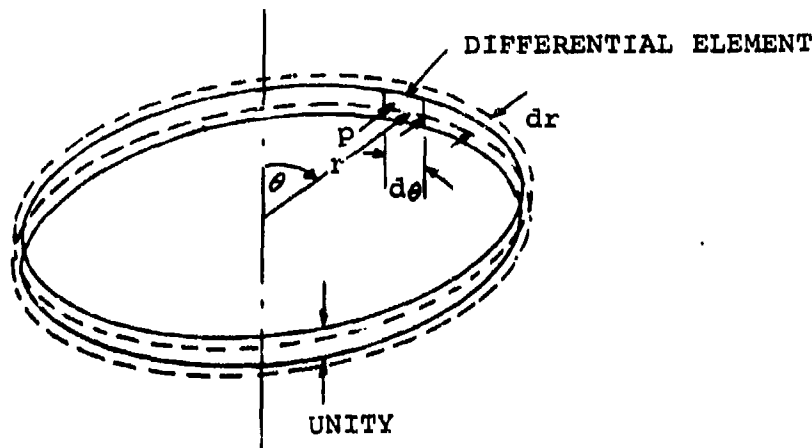


Figure 24. Equatorial, Fabric Hoop at an Intermediate Stage of Inflation

- (2) Since there exists a constant inlet area, the flow rate is limited, whereas the volume to be filled increases on the order of the radius cubed. Therefore, it is reasonable to assume that the differential pressure increases more rapidly when r approaches R than when r is near r_b . In general, this is mathematically stated as,

$$p = k (r - r_b)^n \quad (2)$$

where,

k = a constant

n = a constant exponent

Equation (2) is shown in Figure 25 using several values of n .

A conservatively large value of applied kinetic energy will result from the lower values of n since the areas under these curves are involved. However, $n = 1$ represents a constant rate of increasing pressure that is considered to be unrealistic because of the constant inlet area to volume growth relationship as mentioned above. Therefore, $n = 2$ will be used in the calculations that follow.

- (3) In order for the Ballute to expand, an external, virtual air mass must be displaced. This is implicitly ignored by the conservative assumption that the maximum internal differential pressure developed is equal to the dynamic pressure.

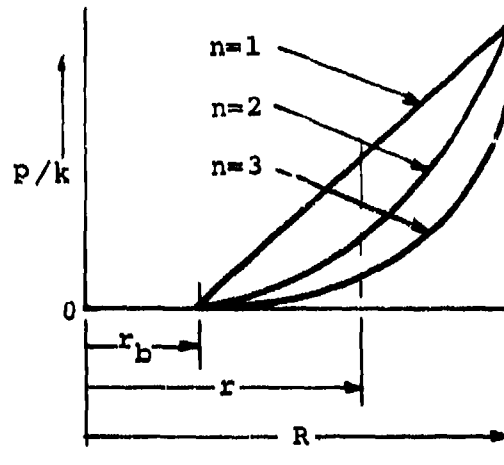


Figure 25. Pressure Increase

The desired pressure function as based upon the preceding discussion may be written as

$$p = q \left(\frac{r - r_b}{R - r_b} \right)^2 \quad (3)$$

Substituting equation (3) into equation (1), integrating and reducing yields,

$$W = \frac{\pi q}{6} (3R^2 - 14 R r_b + 17 r_b^2). \quad (4)$$

Although $r_b = d_i/2 = 4.0$ inches, it is conservative to take $r_b = 0$ so that by equation (4),

$$W \approx \frac{\pi q}{2} R^2. \quad (5)$$

Since the area of the unit width hoop is simply $2 \pi R$, the unit strain energy to be absorbed is given by,

$$u = \frac{W}{2\pi R} = \frac{\pi q R^2}{4 \pi R} = \frac{qR}{4} \quad (6)$$

Recall that $q = 11.45$ pounds per square inch. Hence, the unit strain energies to be absorbed by the 29-inch and by the 41-inch diameter Ballutes becomes, respectively,

$$u = \frac{qR}{4} = \left(\frac{11.45}{4} \right) \left(\frac{29}{2} \right) = 41.5 \text{ inch-pounds per square inch}$$

$$u = \left(\frac{11.45}{8} \right) (41) = 58.7 \text{ inch-pounds per square inch.}$$

Next consider the strain energy-absorbing capacity of the Ballute fabric. The Ballute is constructed so that the warp and fill threads of the single ply fabric are oriented at a 45-degree bias angle with respect to the Ballute's equator. Hence, a typical unit area of an equatorial hoop (refer to Figure 24) is as shown in Figure 26. The total length of warp and fill threads within this unit area absorbs the applied unit strain energy. The following approach is used to determine this length:

- (1) Let n_w and n_f denote the number of warp threads and the number of fill threads per unit width, respectively. For the balanced woven cloth of these Ballutes, $n_w = n_f = n$. The corresponding thread spacing is shown in Figure 26.
- (2) For a load applied normal to a side of the unit area in Figure 26, the number of threads that are loaded is,

$$N = 2 \left(\frac{n}{\sqrt{2}} \right) = n \sqrt{2} \quad \text{threads per inch.} \quad (7)$$

- (3) The length of each loaded thread, such as the length abc, def or gh of Figure 26, is always constant and equal to,

$$l_t = \sqrt{2} \text{ inches per inch.} \quad (8)$$

- (4) Therefore, the total thread length within the unit area of Figure 26 is simply,

$$N l_t = 2n \text{ threads per inch.} \quad (9)$$

The significance of Equation 9 is that the bias construction absorbs twice as much strain energy than a construction having the warp and fill threads oriented parallel and normal to the circumferential direction. Therefore, since the stress-strain curve of Figure 22 applies to each of the warp and to the fill thread sets, the unit strain energies to be absorbed in each are simply the preceding values of u divided by the unit length $N l_t/n$ from Equation (9), i.e.

$$u_t = \frac{nu}{N l_t} = \frac{41.5}{2} = 20.75 \text{ inch-pounds per square inch for the 29-inch diameter Ballute}$$

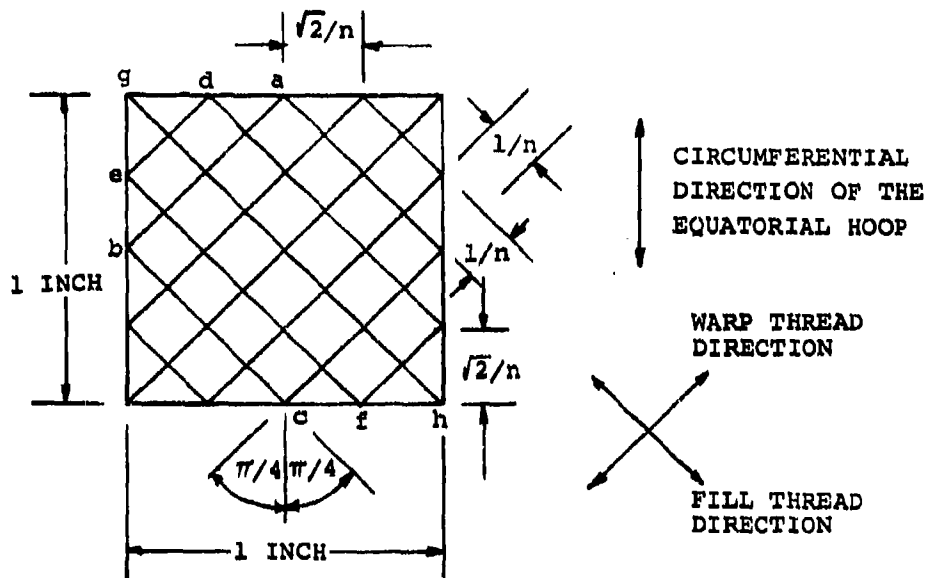


Figure 26. Unit Area of An Equatorial, Fabric Hoop

and,

$$u_t = \frac{58.7}{2} = 29.35 \text{ inch-pounds per square inch for the } 41\text{-inch diameter Ballute}$$

Consider the 41-inch diameter Ballute. A straightforward numerical integration of the area under the stress-strain curve as shown by the shaded area in Figure 22 yields a fabric stress of,

$$\sigma = 706 \text{ pounds per inch.}$$

Following the preceding calculations, the corresponding margin of safety is,

$$\text{M.S.} = \frac{F_{tu}}{(\text{F.S.}) (\sigma)} - 1 = \frac{1500}{(2)(706)} - 1 = \underline{+0.06}$$

For the 1050-pound-per-inch ultimate strength fabric of the 29-inch diameter Ballute, a stress-strain curve is shown in Figure 27. This was based upon that of Figure 22. A numerical integration of the area under this curve as shown by the shaded area in Figure 27 yields a fabric stress of,

$$\sigma = 496 \text{ pounds per inch.}$$

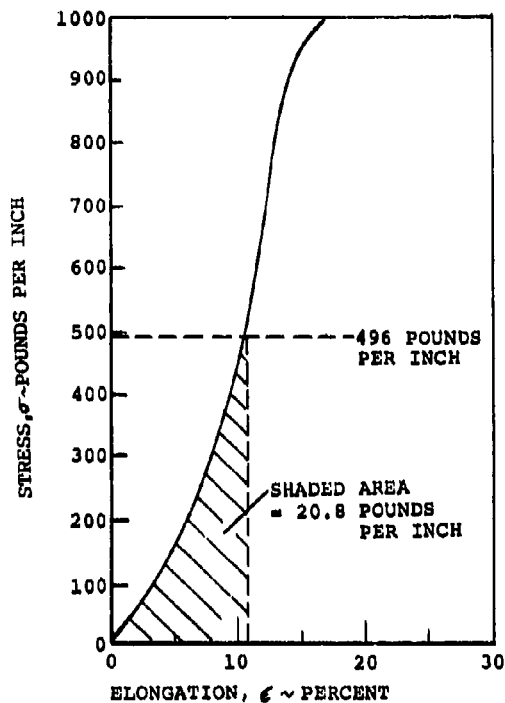


Figure 27. Stress-Strain Curve for the 1050 Pounds Per Inch Fabric (29-Inch Diameter Ballute)

The corresponding margin of safety is,

$$\text{M.S.} = \frac{F_{tu}}{(\text{F.S.}) (\sigma)} - 1 = \frac{1050}{(2) (496)} - 1 = \underline{+0.06}$$

b. Symmetrical Steady-State Stresses

Subsequent to deployment and full inflation of the Ballute to an internal pressure equal to the dynamic pressure, q , the critical pressure vessel, membrane stresses occur. The governing loading condition is the maximum predicted aerodynamic drag and pressure distribution on the 41-inch diameter Ballute as discussed in Section IV, Subsection 3, "Ballute Pressure Distribution."

At the point in time when the pressure distribution of Figure 12 occurs, the Ballute is analyzed as a membrane of revolution loaded symmetrically to its axis; i.e., the longitudinal axis of the bomb. Classical membrane theory such as presented in Chapter 14 of Reference 15 is applied to determine the principal membrane stresses; i.e., N_θ in the meridian direction and N_ϕ in the circumferential direction (refer to Figure 213 of Reference 15).

As a pressure vessel, the Ballute is subjected to a variable differential pressure with respect to the meridian location. In particular, the differential pressure is the internal pressure, q , minus the external pressure that by definition is given by, $c_p q$; i.e.,

$$\text{differential Pressure} = \Delta p = q - c_p q = (1 - c_p)q. \quad (10)$$

In equation 10, positive values of c_p denote external local pressures directed towards the axis of revolution as shown in Figure 28.

The principal membrane stresses are given by Equations 255 and 256 of Reference 15 that become, respectively,

$$2 \pi y N_\theta \cos \phi = R \quad (11)$$

and

$$\frac{N_\phi}{r_1} + \frac{N_\theta}{r_2} = \Delta p, \quad (12)$$

where:

y = radial coordinate of the point of interest as used in Figure 28 in inches

ϕ = meridian slope angle of the point of interest as shown in Figure 28

R = resultant load acting parallel to the axis of revolution on a portion of the shell defined by a parallel circle through the point of interest in pounds.

r_1 and r_2 = the principal radii of curvature at the point of interest in the meridional and in the circumferential directions, respectively.

Therefore, for Δp in units of pounds per square inch, and per the above definitions, the units on N_θ and N_ϕ are stresses in pounds per inch.

(1) The Principal Meridian Stresses, N_θ (Refer to Figure 28)

The critical locations are the forward boundary at Point 1 having $x = 30$ inches and $y = 4$ inches, the Ballute's equator at Point 3 having $x = 0$ and $y = 20.5$ inches, and the aft boundary at Point 6 having $x = 6$ inches and $y = 4$ inches.

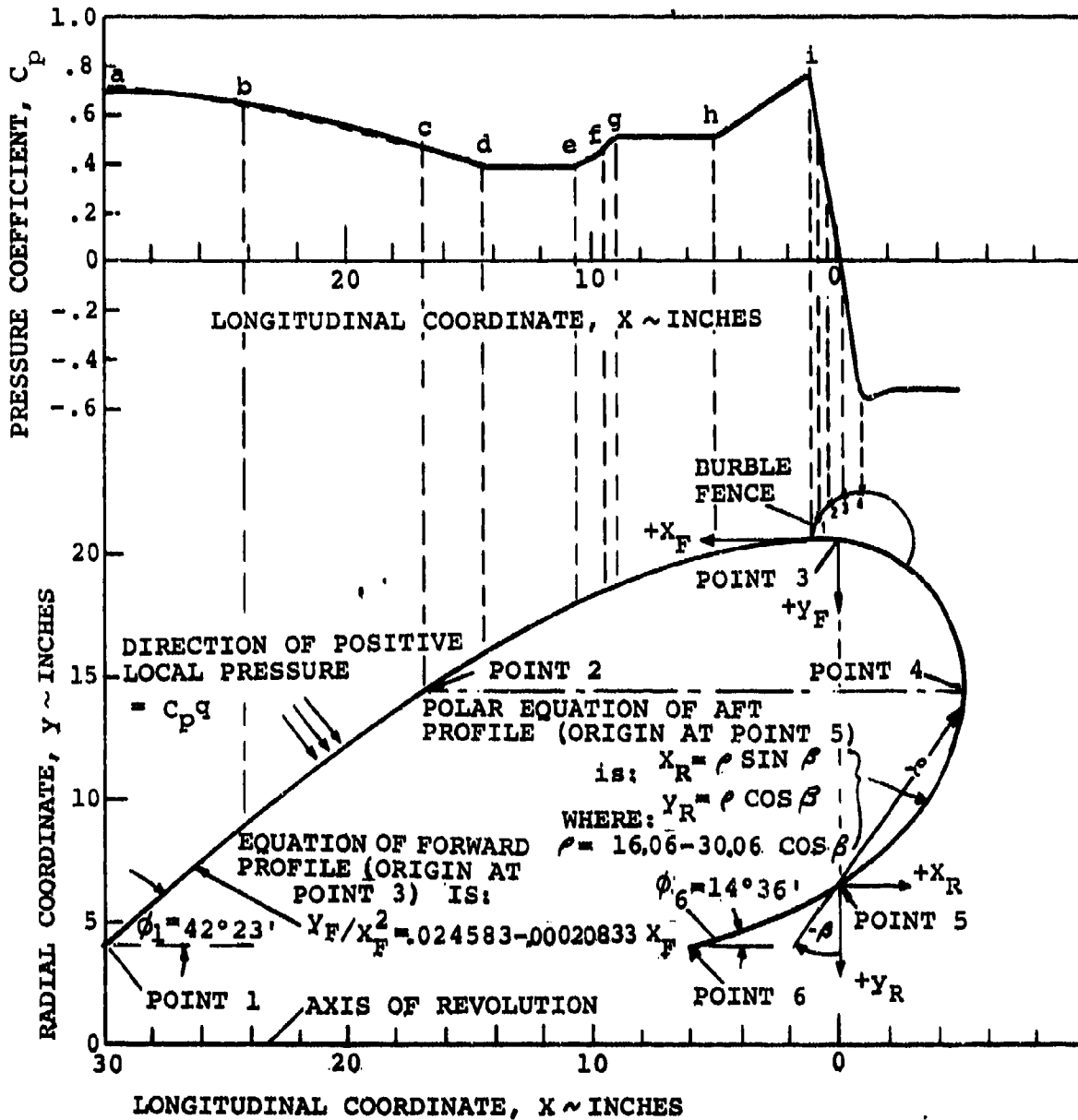


Figure 28. Meridian Profile and Pressures for the 41-Inch Ballute

The meridian stresses of Table I result from the following calculations. The margins of safety in Table I are based upon a factor of safety of F.S. = 2 and an ultimate fabric strength of $F_{tu} = 1500$ pounds per inch. The equation for the margin of safety is,

$$M.S. = \frac{F_{tu}}{(F.S.) N_{\phi}} - 1 = \frac{750}{N_{\phi}} - 1.$$

TABLE I. PRINCIPAL MERIDIAN STRESSES AND MARGINS OF SAFETY

| Location Number (Reference Figure 28) | Meridian Stress N_{ϕ} (pounds per inch) | Margin of Safety M.S. |
|--|--|--------------------------|
| 1 | 395 | +0.89 |
| 3 | 111 | +5.75 |
| 6 | 440 | +0.70 |

Point 6

The slope angle is measured from Figure 28 as

$$\phi_6 = 14^{\circ} 36'.$$

The resultant force, R, is given by the integrated differential pressure acting upon an annular area of outer and inner radii equal to the y values at Point 4 and Point 6, respectively. Point 4 is used since $\phi_4 = 90^{\circ}$ so that,

$$N_{\phi_4} \cos \phi_4 = 0$$

Per the polar equation of the aft profile in Figure 28, the value of y at Point 4 may be calculated as

$$y_4 = 14.5 \text{ inches.}$$

From the pressure distribution of Figure 28, the base drag pressure coefficient is constant at

$$C_p = -0.53.$$

Substitution of these values into Equation (10) and solving for R gives

$$R = (1 - C_p) q \pi (y_4^2 - y_6^2) = (1.53)(11.45) \pi (14.5^2 - 4^2) = \underline{10,690 \text{ pounds.}}$$

Substitution into Equation (11) gives

$$N_{\phi_6} = \frac{10,690}{2 \pi (4) \cos 14^\circ 36'} = 440 \text{ pounds per inch.}$$

Note that the external base drag force on the annular area between 4 and 6 is simply

$$D_{4-6} = \left(\frac{0.53}{1.53} \right) (10,690) = 3703 \text{ pounds.}$$

Point 3

Obviously $\phi_3 = 0$ and the integrated differential pressure acting on the annular area of outer and inner radii equal to the y values at Point 3 and Point 4, respectively, is used in determining the resultant force R . However, the total force R must also include the aerodynamic drag on the burble fence. With reference to Figure 28, the total burble fence drag is considered to be reacted at Point 3.

A variable pressure acts on the forward surface of the burble fence as shown in Figure 28. This surface is divided into four annular rings as indicated. An average value of C_p is applied to each ring and a summation is made in Table II using C_p values and radial coordinates as read from Figure 28.

TABLE II. SUMMATION OF DRAG ON THE FORWARD BURBLE FENCE SURFACE

| Ring Number | Width of Ring, w_R (inches) | Average Radius, r_r of Ring (inches) | Average Value of C_p, C_{p_a} | $(w_R)(r_r)(C_{p_a})$ |
|-------------|-------------------------------|--|---------------------------------|-----------------------|
| 1 | 1 | 21 | 0.6 | 12.6 |
| 2 | 0.5 | 21.75 | 0.34 | 3.7 |
| 3 | 0.3 | 22.15 | 0.12 | 0.8 |
| 4 | 0.2 | 22.4 | -0.29 | <u>- 1.3</u> |
| | | | $\Sigma =$ | 15.8 |

Therefore,

$$2 \pi q \Sigma (w_R)(r_r)(C_{p_a}) = 2 \pi (11.45) (15.8) = 1137 \text{ pounds.}$$

From Figure 28, the rear surface of the burble fence is subjected to the constant base drag pressure coefficient of -0.53 so that the drag force on it is simply,

$$(0.53)(11.45) \pi (\overline{22.5^2} - \overline{20.5^2}) = 1640 \text{ pounds.}$$

Letting D_b denote the total drag force on the burble fences gives,

$$D_b = 1137 + 1640 = 2777 \text{ pounds.}$$

The resultant force that is reacted at Point 3 is

$$\begin{aligned} R &= D_b + (1-C_p) q \pi (y_3^2 - y_4^2) = 2777 + (1.53)(11.45) \pi (\overline{20.5^2} - \overline{14.5^2}) \\ &= 2777 + 11556 = 14,335 \text{ pounds.} \end{aligned}$$

Substitution into Equation (11) gives

$$N_{\phi_3} = \frac{14,335}{2 \pi (20.5)} = 111 \text{ pounds per inch.}$$

Note that the external base drag force on the annular area between locations 3 and 4 is

$$D_{3-4} = \left(\frac{0.53}{1.53} \right) (11556) = 4004 \text{ pounds.}$$

Point 1

The total aerodynamic drag force applied to the Ballute and its burble fence must be reacted at the two boundary attachments, namely locations 1 and 6 of Figure 28. The reaction at Point 6 is already known from the meridian stress at point 6; i.e. N_{ϕ_6} . This reactive force is

$$\begin{aligned} F_{x6} &= 2 \pi y_6 N_{\phi_6} \cos \phi_6 \\ &= 2 \pi (4)(440) \cos 14^\circ 36' = 10,690 \text{ pounds.} \end{aligned}$$

The total applied drag force may be expressed as (refer to Figure 28)

$$D = D_{1-3} + D_b + D_{3-4} + D_{4-6}. \quad (13)$$

In equation (13), only the term D_{1-3} is yet to be determined. This represents the external aerodynamic drag force acting upon the forward surface of the Ballute.

In Figure 28, consider the pressure coefficient distribution between Locations 1 and 3 on the Ballute. This curve may be closely approximated by a series of eight straight lines between the points a through i as indicated. The corresponding locations of these points on the surface of the Ballute are indicated by the intercepts of the vertical dashed lines in Figure 28. The radial coordinate of each of these intercepts is taken from Figure 28 and used to define the inner and outer radii of each of the eight annular areas upon which the average pressure coefficient is applied. This summation technique is similar to that used for the burble fence in Table II. For example, the drag force on the ring between Points c and d of Figure 28 is given by

$$\begin{aligned} D_{cd} &= \frac{1}{2} (C_{p_c} + C_{p_d}) q \pi (y_d^2 - y_c^2) \\ &= \frac{\pi}{2} q (0.46 + 0.38) (\overline{16}^2 - \overline{14.5}^2) = 19.22 \pi q. \end{aligned} \quad (14)$$

Calculations similar to that of equation (14) are performed for each of the eight rings in Table III. A cumulative total is made to indicate the increasing drag force from Point 1 towards Point 3.

Therefore, the total drag on the forward surface of the Ballute is (using the last value in Table III)

$$D_{1-3} = 209.35 \pi q = 209.35 \pi (11.45) = 7530 \text{ pounds.}$$

The total drag force on the Ballute and its burble fence is given by substituting all of the preceding drag values into equation (13); i.e.,

$$D = 7530 + 2777 + 4004 + 3703 = 18,014 \text{ pounds.}$$

Consideration of equilibrium of forces in the longitudinal direction yields the reactive force at the forward Ballute boundary attachment as

$$F_{x1} = D - F_{x6} = 18,014 - 10,690 = 7324 \text{ pounds.}$$

The slope angle at Point 1 may either be measured in Figure 28 or determined by differentiation of the given equation of the forward profile as

$$\theta_1 = 42^\circ 23'.$$

TABLE III. SUMMATION OF DRAG ON THE FORWARD BALLUTE SURFACE

| Location Number | Pressure Coefficient | Average Pressure Coefficient C_{pav} | Radius y (inches) | Area of Ring Divided by π . A/π (sq. in.) | $(A/\pi) C_{pav}$ (Square Inches) | $\Sigma (A/\pi) C_{pav}$ (Square Inches) |
|-----------------|----------------------|--|---------------------|---|-----------------------------------|--|
| a | 0.72 | 0.6 | 4 | 65 | 44.53 | 44.53 |
| b | 0.65 | 0.55 | 9 | 129.25 | 71.09 | 115.62 |
| c | 0.46 | 0.42 | 14.5 | 65.75 | 19.22 | 134.84 |
| d | 0.38 | 0.38 | 16 | 68 | 25.84 | 160.68 |
| e | 0.38 | 0.405 | 18 | 18.25 | 7.39 | 168.07 |
| f | 0.43 | 0.465 | 18.5 | 7.44 | 3.46 | 171.53 |
| g | 0.5 | 0.5 | 18.7 | 50.31 | 25.16 | 196.69 |
| h | 0.5 | 0.625 | 20 | 20.25 | 12.66 | 209.35 |
| i | 0.75 | | 20.5 | | | |

The desired meridian stress is [refer to Equation (11)]

$$N_{\theta_1} = \frac{F x_1}{2 \pi y_1 \cos \theta_1} = \frac{7324}{2 \pi (4) \cos 42^\circ 23'} = 395 \text{ pounds per inch.}$$

(2) The Principal Circumferential Stresses, N_{θ}

Having determined the meridian stresses at Points 1, 3, and 6, the corresponding circumferential stresses may be calculated per Equation (12). Here, the differential pressure is given by substituting the proper values for C_p from Figure 28 into Equation (10) along with $q = 11.45$ pounds per square inch as previously used.

The principal radii of curvature; i.e., r_1 and r_2 , are shown in Figure 213 of Reference 15. Figure 29 is based upon the shape of Figure 28 and is sketched to indicate these radii of curvature. r_1 and r_2 are in the meridian plane and perpendicular to the meridian plane, respectively. r_2 is easily obtained from geometry since the center lies on the axis of revolution.

In general, from Figure 29,

$$r_2 = y \sec \theta \tag{15}$$

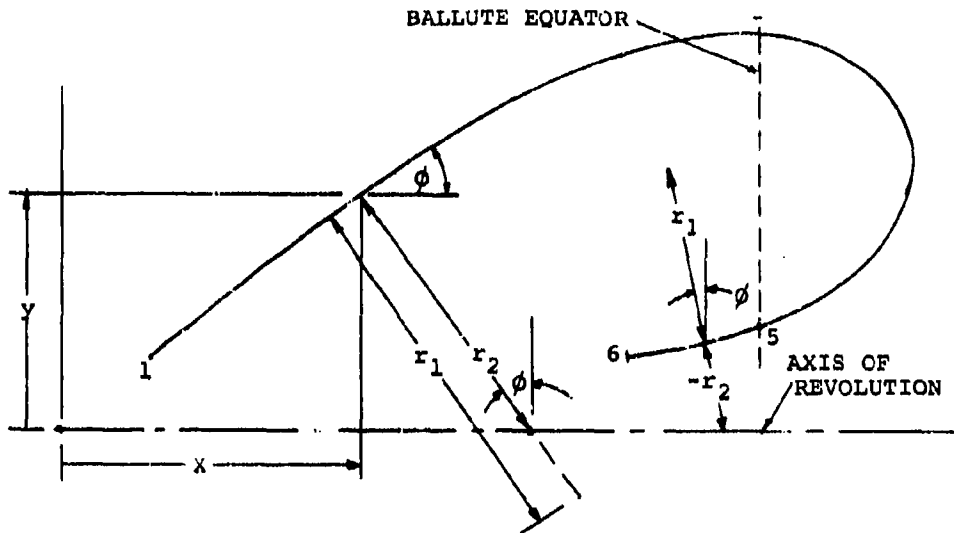


Figure 29. Ballute Profile Showing Principal Radii of Curvature

In calculus, it is shown that the expression for the meridian radius of curvature is

$$r_1 = \frac{[1 + (dy/dx)^2]^{3/2}}{d^2y/dx^2}$$

Of course, $dy/dx = \tan \phi$ so that

$$r_1 = \frac{\sec^3 \phi}{d^2y/dx^2} \quad (16)$$

The second derivative of the equation that describes the forward surface of the Ballute (see Figure 28) is

$$d^2y/dx^2 = 2 (0.024583) - 6 (0.00020833) x_F. \quad (17)$$

The second derivative of the parametric equations that describe the aft surface of the Ballute is derived as follows:

$$dy/d\beta = -60.12 \sin \beta \cos \beta - 16.06 \sin \beta \quad (18)$$

$$dx/d\beta = 30.06 (\sin^2 \beta - \cos^2 \beta) + 16.06 \cos \beta \quad (19)$$

$$d^2y/d\beta^2 = 60.12 (\sin^2 \beta - \cos^2 \beta) - 16.06 \cos \beta \quad (20)$$

$$d^2x/d\beta^2 = 120.24 \sin \beta \cos \beta - 16.06 \sin \beta \quad (21)$$

From any advanced calculus text, it may be shown that

$$d^2y/dx^2 = \frac{(dx/d\beta)(d^2y/d\beta^2) - (dy/d\beta)(d^2x/d\beta^2)}{(dx/d\beta)^3} \quad (22)$$

Point 6

From Figure 28, $\theta_6 = 14^\circ 36'$, $y_6 = 4$ inches, and $\beta = \tan^{-1} \left(\frac{-6}{6.5 - 4} \right)$
 $= \tan^{-1} - 2.4 = -67^\circ 23'$,

$$\sin \beta = -0.9231, \quad \cos \beta = 0.38456.$$

Substituting these values into Equations (16) through (22) and simplifying yields

$$d^2y/dx^2 = 0.097638 \text{ (inches)}^{-1}$$

$$r_1 = \frac{\sec^3 14.6^\circ}{0.097638} = 11.3 \text{ inches.}$$

Per Equation (15),

$$r_2 = -y_6 \sec \theta = -4 \sec 14.6^\circ = -4.134 \text{ inches.}$$

From Table I, $N_{\theta_6} = 440$ pounds per inch

From Figure 28, $C_p = -0.53$ so that in Equation (10)

$$\Delta p = (1.53) (11.45) = 17.519 \text{ pounds per square inch.}$$

Substituting the above values into Equation (12), and solving for N_{θ} gives

$$\begin{aligned} N_{\theta_6} &= r_2 \left(\Delta p - \frac{N_{\theta}}{r_1} \right) \\ &= -4.134 \left(17.519 - \frac{440}{11.3} \right) = 88.5 \text{ pounds per inch.} \end{aligned}$$

The margin of safety at Point 6 for F.S. = 2 and for $F_{tu} = 1500$ pounds per inch is

$$\text{M.S.} = \frac{1500}{(2) (88.5)} - 1 = 47.47.$$

Point 3

The following values are taken from Figure 28:

$$C_p = 0.76 \text{ at point i of the pressure curve}$$

$$\theta = 0 \text{ degrees}$$

$$x_{F3} = 0 \text{ inches} \quad y_{F3} = 20.5 \text{ inches.}$$

Substituting into Equations (10), (17), (16), and (15) gives

$$\Delta p = (1 - 0.76) (11.45) = 2.75 \text{ pounds per square inch,}$$

$$d^2y/dx^2 = 2 (0.024583) = 0.049166 \text{ (inches)}^{-1},$$

$$r_1 = \frac{1}{0.049166} = 20.34 \text{ inches,}$$

$$r_2 = y_{F3} = 20.5 \text{ inches.}$$

From Table I, $N_{\theta_3} = 111$ pounds per inch.

Substituting these values into Equation (12) and solving for N_0 gives

$$N_{0_3} = 20.5 \left(2.75 - \frac{111}{20.34} \right) = -55.4 \text{ pounds per inch.}$$

Note that this negative sign indicates a compressive stress which tends to wrinkle the fabric since it has no compressive resistance. In order to prevent this situation, the forward profile is revised with a fourth order curve in replacement of the third order curve of Figure 28. The equation of this revised forward profile was determined by trial and error to be

$$y_F/x_F^2 = 10^{-2} + 7.639 \times 10^{-4} x_F - 1.62044 \times 10^{-5} x_F^2 \quad (23)$$

The meridian radius of curvature at Point 3 is next determined for this revised shape and the corresponding circumferential stress is calculated using the preceding methods:

$$\begin{aligned} \tan \phi &= dy_F/dx_F = (2 \times 10^{-2} + 3 \times 7.639 \times 10^{-4} x_F - 4 \times 1.62044 \times 10^{-5} x_F^2) x_F \\ &= (2 + 0.22917 x_F - 0.00648176 x_F^2) \frac{x_F}{100} \end{aligned} \quad (24)$$

$$d^2y_F/dx_F^2 = (2 + 0.45834 x_F - 0.0194453 x_F^2) \times 10^{-2} \quad (25)$$

At Point 3, $x_F = 0$ so that by Equation (16),

$$r_1 = \frac{1}{d^2y_F/dx_F^2} = \frac{1}{0.02} = 50 \text{ inches.}$$

Substituting the proper values into Equation (12) and solving for N_0 gives

$$N_{0_3} = 20.5 \left(2.75 - \frac{111}{50} \right) = 10.9 \text{ pounds per inch.}$$

Point 1

Here, $x_F = 30$ inches (refer to Figure 28). Substituting this value into Equation 24 and solving for the slope angle gives

$$\phi_1 = \tan^{-1} 0.91245 = 42^\circ 23'.$$

This agrees with the angle of Figure 28. Hence, the meridian stress at Point 1 remains unchanged from that previously determined for the third degree curve.

From Equations (15), (25) and (16),

$$r_2 = 4 \text{ sec } 42^\circ 23' = 5.45 \text{ inches,}$$

$$d^2yF/dx^2 = -0.0175057,$$

$$r_1 = -144.5 \text{ inches.}$$

At Point a on the pressure plot of Figure 28, $C_p = 0.7$ so that from Equation (10),

$$\Delta p = (1 - 0.7)(11.45) = 3.435 \text{ pounds per square inch.}$$

From Page 43,

$$N_{\theta_1} = 395 \text{ pounds per inch}$$

Substituting the above values into Equation (12) and solving for N_{θ} gives

$$N_{\theta_1} = 5.45 \left(3.435 + \frac{395}{144.5} \right) = 33.6 \text{ pounds per inch.}$$

The positive values of N_{θ_1} and N_{θ_3} show that the forward Ballute profile is stable, i.e., unwrinkled.

3. METAL ANALYSIS

a. General

Five principal metal components, as denoted in Figure 2, are structurally analyzed herein. The resulting calculated margins of safety are presented in Table IV. These margins are based upon yield and ultimate factors of safety of 1.15 and 1.5, respectively.

b. Loads

The three design loading conditions are discussed in Section IV. Cases 1 and 2 occur at a 20-degree angle of attack and therefore yield the critical side loading conditions. Since the Ballute is never deployed under the

TABLE IV. SUMMARY OF THE CALCULATED MARGINS OF SAFETY FOR THE METAL COMPONENTS

| Component (Reference Figure 2) | Refer to Figure Numbers | Critical Loading Condition (Reference Pages 15, 17, and 18, Section IV) | Governing Stress Condition | Calculated Margin of Safety | Reference Page Number |
|--|-------------------------------|---|------------------------------------|-----------------------------------|-----------------------------|
| 3. Forward Ballute Clamp Ring MS 3519-320 Screws | 2 | Case 3 | Single Shear | +0.19 | 50 |
| 9. Tail Panel (Fin) 356-T6 Aluminum | 2, 8, 11 | Case 1 | Bending | +6.82 | 51 |
| 6. Rear Plate of the Release Mechanism AISI 1020 Steel | 2, 6 | Case 3 | Bending | +0.30 | 52 |
| 2. Canister Assembly Shell | 2,5,30,31 | Case 2 | Bending | +0.98 | 56 |
| 356-T6 Aluminum Aft Ring | 5,31,32,33 | Case 2 | Bending | +0.29 | 61 |
| 356-T6 Aluminum Forward Joint | 2,5,31,34 | Case 2 | Combined Tension and Bending | +0.06 | 64 |
| 1. Clamp Band Assembly Clamp Ring | 2,4,34,35 | Case 2 | Combined Tension and Bending | +2.29 | 66 |
| 4142-II Steel Clamp Band | 2,4,35,36 | Case 2 | Tension | -0.02 | 68 |
| 4130 Steel Gusseted Clamp Band Area | 4,38,39 | Case 2 | Combined Tension and Bending | +0.08 | 73 |
| MS24678-47 Screws | 4,38 | Case 2 | Tension | +0.30 | 73 |

conditions of Case 1, the largest side loads that are applied to the Ballute and that are transmitted to the canister will occur under Case 2 only. Case 1 is used only for analysis of the tail panels (fins) where the maximum panel force is 475 pounds for the 1-1/2 caliber tail panel (refer to Page 15).

The maximum drag force of 18,014 pounds (refer to Page 42) occurs under Case 3 at a zero angle of attack as given in Section IV, Page 17. This has been used in the fabric analysis section and applies herein to the analysis of the forward Ballute clamp ring and the rear plate (refer to Figures 2 and 6). This axial load is not critical to the canister and its components since the bending load due to the case 2 side loading was found to govern.

c. Analysis

(1) Forward Ballute Clamp Ring. The location of this ring is sketched in Figure 2. The ring is split in two halves and is located internal to the canister. The cylindrical fabric sleeve of the Ballute is clamped between this ring and the canister to provide the reaction to the entire Ballute drag force of $D = 18,014$ pounds. The critical components are the screws that connect the clamp ring halves to the canister. There are a total of ten screws used; i.e., $N = 10$. Each of these are loaded in single shear to a limit load level of

$$V = \frac{D}{N} = \frac{18014}{10} = 1801.4 \text{ pounds per screw.}$$

Standard, MS 35191-320 screws are used that have an ultimate single shear strength of

$$V_u = 3240 \text{ pounds per screw.}$$

For an ultimate factor of safety of F.S. = 1.5, the margin of safety is

$$\text{M.S.} = \frac{V_u}{(\text{F.S.})(V)} - 1 = \frac{3240}{(1.5)(1801.4)} - 1 = +0.19.$$

(2) Tail Panel (Fin). This component is sketched in Figure 2. It is an integral part of the canister. This is a casting of 356-T6 aluminum alloy for which the tensile yield and ultimate strengths are given on Page 3-275 of Reference 16 as, respectively

$$F_{ty} = 20,000 \text{ pounds per square inch}$$

$$F_{tu} = 30,000 \text{ pounds per square inch.}$$

As previously noted, the maximum force that is applied normal to the surface of the fin is, $P = 475$ pounds for the 1-1/2 caliber tail, Case 1, Page 15 of Section IV.

The fin is analyzed as a uniformly loaded, cantilevered beam with maximum bending stresses occurring at the root chord cross section. The length of this beam is calculated from Figure 11 as

$$l = \frac{1}{2} (\text{span} - 8.75) = \frac{1}{2} (16 - 8.75) \approx 3.63 \text{ inches.}$$

Also per Figure 11, the root chord of the 1-1/2 caliber tail is

$$C_R = (1.5) (10.75) = 16.12 \text{ inches.}$$

The thickness of the fin at its root is given in Figure 8 as $t = 0.38$ inches.

Therefore, from any standard structural technology handbook, the bending stress is simply

$$\sigma_b = \frac{3 P l}{C_R t^2} = \frac{3(475)(3.63)}{(16.12)(0.38)^2} = 2,222 \text{ pounds per square inch.}$$

The corresponding margins of safety for yield and ultimate conditions using factors of safety of 1.15 and 1.5, respectively, are calculated below:

For yield,

$$\text{M.S.} = \frac{F_{ty}}{(\text{F.S.})(\sigma_b)} - 1 = \frac{20,000}{(1.15)(2,222)} - 1 = +6.82.$$

For ultimate,

$$\text{M.S.} = \frac{F_{tu}}{(\text{F.S.})(\sigma_b)} - 1 = \frac{30,000}{(1.5)(2,222)} - 1 = +8.00.$$

(3) Rear Plate. This plate is part of the release mechanism of Figures 2 and 6. Its radius and thickness are, respectively,

$$a = \frac{1}{2} (8.32) = 4.16 \text{ inches}$$

$$t = 0.125 \text{ inches}$$

The plate serves as a closure for the rear surface of the Ballute. As such, it is subjected to the maximum differential pressure that occurs for the aerodynamic Case 3. This pressure is given by substituting the base drag pressure coefficient from Figure 28 into Equation (10); i.e.,

$$\Delta p = (1 - C_p) q = (1.53)(11.45) = 17.52 \text{ pounds per square inch.}$$

The plate is clamped around its outer edge to the cylindrical fabric sleeve of the Ballute. This provides a simply supported edge reaction to the uniformly applied pressure force so that Case 1, Page 194 of Reference 17 may be directly applied to determine the maximum bending stress; i.e.,

$$\begin{aligned} \sigma_b &= \frac{3 \Delta p a^2}{8t^2} (3 + \mu) = \frac{3 (17.52) (4.16)^2}{8 (0.125)^2} (3 + 0.3) \\ &= 24,000 \text{ pounds per square inch.} \end{aligned}$$

In the above equation, $\mu = 0.3$ is a good, average value of Poisson's ratio for steel.

The material is low carbon AISI 1020 steel for which the yield and ultimate tensile strengths are taken from Page 2-5 of Reference 16 as

$$F_{ty} = 36,000 \text{ pounds per square inch,}$$

$$F_{tu} = 55,000 \text{ pounds per square inch.}$$

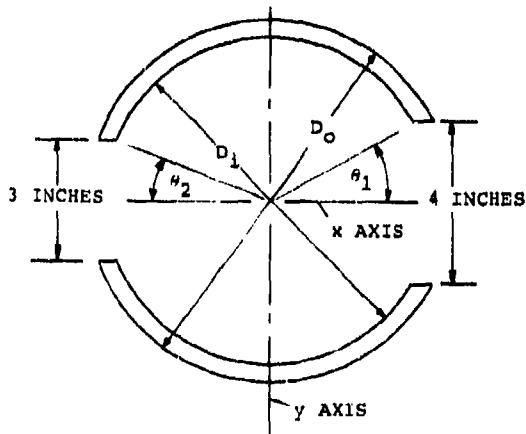
The corresponding margins of safety are, respectively,

$$\text{M.S.} = \frac{36,000}{(1.15)(24,000)} - 1 = + 0.30 \text{ on yield,}$$

$$\text{M.S.} = \frac{55,000}{(1.5)(24,000)} - 1 = + 0.52 \text{ on ultimate.}$$

(4) Canister Assembly (Reference Figures 2 and 5)

(a) Canister Shell. First consider the maximum drag load of 18,014 pounds of Case 1 that subjects the minimum cross sectional area of the canister to pure tensile stresses. This cross section is located at the two access holes and is sketched in Figure 30 using the dimensions of Figure 5.



Inner diameter, $D_1 = 8$ inches

Outer diameter, $D_0 = 8.75$ inches

Central, cut-out angles are,

$$\theta_1 = \sin^{-1} \left(\frac{2}{4} \right) = 30 \text{ degrees}$$

$$\theta_2 = \sin^{-1} \left(\frac{1.5}{4} \right) = 22 \text{ degrees}$$

Figure 30. Cross Section of Canister Shell at Access Holes

Let A_t denote the tensile area of Figure 30.

This is easily calculated as,

$$\begin{aligned} A_t &= \left(1 - \frac{\theta_1 + \theta_2}{180} \right) \frac{\pi}{4} (D_0^2 - D_1^2) \\ &= \left(1 - \frac{52}{180} \right) \frac{\pi}{4} (76.563 - 64) = 7 \text{ square inches.} \end{aligned}$$

The tensile stress is then

$$\sigma_t = \frac{D}{A_t} = \frac{18,014}{7} = 2,573 \text{ pounds per square inch.}$$

This stress is less than the bending stress due to the side loading of Case 2 that is calculated as follows:

From Section IV, Subsection 5, the normal or side load is $F_N = 3,420$ pounds and acts at the center of pressure that is located 5.4 inches aft of the Ballute base. This is shown in Figure 31.

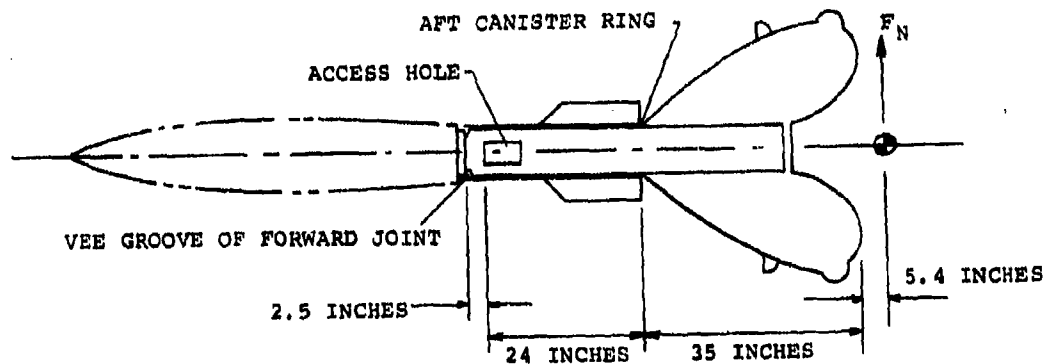


Figure 31. Location of the Normal Force, F_N

The critical bending section is also that of Figure 30. The maximum bending moment on this section occurs at the forward end of the largest access hole located 24 inches from the aft ring of the canister shell as shown in Figure 31. The maximum bending moment for a 3420-pound side force located per Figure 31 is then

$$M_{MAX} = (24 + 35 + 5.4)(3,420) = 220,248 \text{ inch-pounds.}$$

This bending moment far exceeds that which can be transmitted by the inflated Ballute. The design bending moment will be reduced to agree with the maximum estimated value of F_N for which the Ballute will remain essentially undeformed from its symmetrically inflated shape.

Under side loading, the Ballute is critical at its minimum cross section located at the aft ring of the canister in Figure 31. The bending moment at this section is given by

$$M_B = (35 + 5.4) F_N = 40.4 F_N. \quad (26)$$

The maximum value of M_B is taken as that which will completely collapse this cylindrical cross section. The contractor has theoretically derived and experimentally verified that a pressurized fabric cylinder subjected to pure bending will collapse at somewhat less than twice the bending moment required for incipient wrinkling at the extreme fiber on the compression side of the circular cross section. Let M_w denote this first wrinkling moment, then the above statement is expressed as

$$M_B = 2 M_w \quad (27)$$

The membrane bending load is given by the classical flexural equation as

$$N_B = \frac{M_w c}{I} \quad \text{in pounds per inch} \quad (28)$$

where, for a circular cross section,

$$c = D_1/2 \text{ in inches and}$$

$$I = \pi/8 D_1^3 \text{ in cubic inches.}$$

Therefore,

$$N_B = \frac{4 M_w}{\pi D_1^2} \quad (29)$$

A conservatively high value of M_w results by setting N_B of Equation (29) equal to the maximum longitudinal tensile membrane force due to the 10,250-pound drag load of Case 2 (refer to Subsection 5 of Section IV). Such an equation means that the bending stress on the compression side will exactly overcome the tensile stress due to aerodynamic drag thus causing incipient wrinkling. Therefore,

$$\frac{4 M_w}{\pi D_1^2} = \frac{D}{\pi D_1}$$

or,

$$M_w = \frac{D_1}{4} D = \left(\frac{8}{4}\right) (10,250) = 20,500 \text{ inch-pounds.}$$

Substituting into Equation (27) gives

$$M_B = 41,000 \text{ inch-pounds.}$$

Substituting into Equation (26) gives a maximum possible side force of

$$F_N = \frac{41,000}{40.4} = 1015 \text{ pounds.}$$

The corresponding bending moment on the critical canister shell cross section of Figures 30 and 31 is then

$$M_{MAX} = (24 + 35 + 5.4) (1015) = 65,366 \text{ inch-pounds.}$$

A conservatively small value of the classically defined section modulus (I/c) is given by assuming a 4-inch access hole on each side of the cross section in Figure 30. The moments of inertia about the x and about the y axes of Figure 30 are, respectively,

$$I_x = 81.68 \text{ inches to the fourth power,}$$

$$I_y = 33.89 \text{ inches to the fourth power.}$$

These were calculated by the formulas on Page 4.1.8 of Reference 18 as follows:

$$\begin{aligned} I_x &= \frac{1}{32} \left(\frac{\pi}{2} - \theta_1 \right) (D_o^4 - D_i^4) \left[1 + \frac{\sin \left(\frac{\pi}{2} - \theta_1 \right) \cos \left(\frac{\pi}{2} - \theta_1 \right)}{\frac{\pi}{2} - \theta_1} \right] \\ &= \left(\frac{8.75^4 - 8^4}{32} \right) \left(\frac{\pi}{2} - \frac{30\pi}{180} + \sin \frac{\pi}{3} \cos \frac{\pi}{3} \right) \\ &= (55.182) \left(\frac{\pi}{3} + 0.433 \right) = 81.68 \text{ inches to the fourth power} \end{aligned}$$

$$I_y = \frac{1}{32} \left(\frac{\pi}{2} - \theta_1 \right) (D_o^4 - D_i^4) \left| 1 - \frac{\sin \left(\frac{\pi}{2} - \theta_1 \right) \cos \left(\frac{\pi}{2} - \theta_1 \right)}{\frac{\pi}{2} - \theta_1} \right|$$

$$= (55.182) \left(\frac{\pi}{3} - 0.433 \right) = 33.89 \text{ inches to the fourth power.}$$

The minimum section modulus obviously corresponds to the I_y and is given as (refer to Figure 30)

$$\frac{I}{c} = \frac{2 I_y}{D_o \cos \theta_1} = \frac{2 (33.89)}{(8.75) (0.866)} = 8.945 \text{ cubic inches.}$$

Substituting this value of the section modulus along with the preceding value of the maximum bending moment into the classical flexural equation yields the desired bending stress

$$\sigma_b = M_{MAX} \frac{C}{I} = \frac{65,366}{8.945} = 7,308 \text{ pounds per square inch.}$$

This bending stress must be combined with the longitudinal tensile stress due to the 10,250-pound drag load of Case 2. The net tensile area was previously calculated as $A_t = 7$ square inches. Hence, the longitudinal tensile stress is

$$\sigma_t = \frac{10,250}{7} = 1,464 \text{ pounds per square inch}$$

The combined stress is

$$\sigma = \sigma_b + \sigma_t = 7,308 + 1,464 = 8,772 \text{ pounds per square inch.}$$

The material is the 356-T6 aluminum alloy casting so that the margins of safety on yield and ultimate conditions are, respectively (refer to the tail panel analysis of Paragraph 3-c-(2) of this section).

$$\text{M.S.} = \frac{20,000}{(1.15)(8,772)} - 1 = +0.98 \text{ on yield,}$$

$$\text{M.S.} = \frac{30,000}{(1.5)(8,772)} - 1 = +1.27 \text{ on ultimate.}$$

(b) Aft Canister Ring. The aft ring is an integral part of the canister casting. It is located as sketched in Figure 31. A cross section of this ring region of the canister is shown in Figure 32 along with an end view of the plane of the ring that indicates the distribution of the applied load.

The total load is applied in the plane of the ring and is equal to the maximum possible side force of $F_N = 1015$ pounds as previously calculated. Since the cylindrical fabric sleeve of the Ballute is not attached to the aft ring, it can only transfer the side load to the ring by bearing against the inner surface. This bearing load is considered to be distributed as a cosine function over half of the ring's mean circumference as shown in Figure 32.

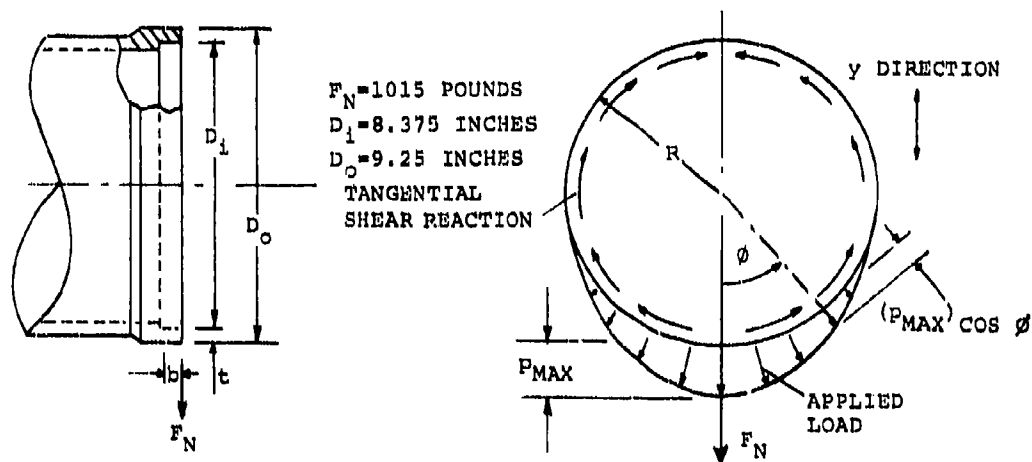


Figure 32. Section of Aft Canister Ring and Applied Shear Load

Let p_{MAX} denote the maximum distribution load at $\phi = 0$ degrees in Figure 32. Its relationship to F_N is determined by integrating the forces in the y direction of Figure 32 and equating to F_N ; i.e.,

$$2 R p_{MAX} \int_0^{\frac{\pi}{2}} \cos^2 \phi \, d\phi = F_N.$$

Integrating this equation gives

$$p_{MAX} = \frac{2 F_N}{\pi R} \text{ pounds per inch.} \quad (30)$$

In Equation(30), R is the mean radius of the ring that from Figure 32 is equal to

$$R = \frac{1}{4} (D_o + D_i) = \frac{1}{4} (9.25 + 8.375) = 4.406 \text{ inches.}$$

Substituting this value along with the value of F_N into Equation(30) gives

$$P_{MAX} = \frac{2}{\pi} \left(\frac{1015}{4.406} \right) = 146.7 \text{ pounds per inch.}$$

The internal in-the-plane of the ring forces and bending moments caused by a cosine loading and tangential shear reaction are given in Case 18 of Reference 19. This is directly applicable to the case of Figure 32. From this reference, two locations on the ring must be checked for critical stresses; i.e.,

At $\theta = 0$ degrees

The bending moment is

$$\begin{aligned} M_o &= 0.06832 P_{MAX} R^2 \\ &= (0.06832)(146.7)(4.406)^2 = 194.6 \text{ inch pounds.} \end{aligned}$$

The circumferential force is compressive and equal to

$$N_o = -0.75 P_{MAX} R = (-0.75)(146.7)(4.406) = -484.8 \text{ pounds.}$$

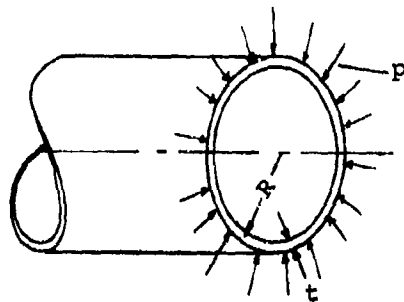
At $\theta = 90$ degrees

The bending moment is

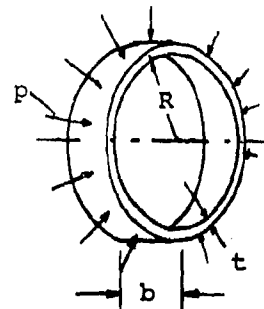
$$M_{90} = 0.07438 (146.7)(4.406)^2 = 211.8 \text{ inch pounds.}$$

The circumferential force is tensile and equal to

$$N_{90} = 0.3927 (146.7)(4.406) = 253.8 \text{ pounds.}$$



(A) RADIALLY LOADED CYLINDER



(B) RADIALLY LOADED RING

Figure 33. Equivalence Between Radially Loaded Cylinder and Ring

In order to evaluate the section modulus (I/c) and the cross sectional area (A_c) of this aft ring, an effective width denoted by the symbol b in Figure 32 must be estimated. This is done by equating the circumferential stress in a radially loaded ring of width b and thickness t to the maximum circumferential stress in a cylinder subjected to a radial load of equal magnitude as applied at the end of the cylinder. This approach is considered representative of the case of Figure 32. These two cases are sketched in Figure 33.

The symbols of Figure 33 are:

R = mean radius of the ring and cylinder in inches

p = radial load applied to ring and cylinder in pounds per inch

t = wall thickness of ring and cylinder in inches

b = width of the ring in inches

The maximum circumferential stress for the cylinder of Figure 33 is given in Case 10, Page 271 of Reference 17 as

$$\sigma_{MAX} = \frac{-2 p R}{t} \sqrt[4]{\frac{3(1-\mu^2)}{R^2 t^2}} \text{ pounds per square inch. (31)}$$

The circumferential stress in the ring of Figure 33 is given by Case 1, Page 268 of Reference 17, as

$$\sigma = \frac{-p R}{b t} \text{ pounds per square inch. (32)}$$

Setting $\sigma = \sigma_{MAX}$ per Equations (31) and (32), substituting $\mu = 0.3$ as a representative value of Poisson's ratio for aluminum, and solving for the effective width yields

$$b = 0.389 \sqrt{R t} \quad \text{inches.} \quad (33)$$

From Figure 32,

$$R = \frac{1}{4} (D_o + D_i) = \frac{1}{4} (9.25 + 8.375) = 4.406 \text{ inches,}$$

$$t = \frac{1}{2} (D_o - D_i) = \frac{1}{2} (9.25 - 8.375) = 0.437 \text{ inches.}$$

Therefore, from Equation (33),

$$b = 0.389 \sqrt{(4.406)(0.437)} = 0.540 \text{ inches.}$$

The desired cross-sectional area and section modulus of the ring may now be calculated; i.e.,

$$A_c = b t = (0.54)(0.437) = 0.236 \text{ square inches,}$$

$$\frac{I}{c} = \frac{b t^2}{6} = (0.236) \left(\frac{0.437}{6} \right) = 0.01719 \text{ cubic inches.}$$

For the preceding calculated forces and moments, the combined stresses at $\theta = 0$ and at $\theta = 90$ degrees become

At $\theta = 0$ degrees

$$\begin{aligned} \sigma_o &= \frac{N_o}{A_c} - \frac{M_o c}{I} = -\frac{484.8}{0.236} - \frac{194.6}{0.01719} \\ &= -2,054 - 11,320 = -13,374 \text{ pounds per square inch (compression)} \end{aligned}$$

At $\theta = 90$ degrees

$$\begin{aligned} \sigma_{90} &= \frac{N_{90}}{A_c} + \frac{M_{90} c}{I} = \frac{253.8}{0.236} + \frac{211.8}{0.01719} \\ &= 1075 + 12,321 = 13,396 \text{ pounds per square inch (tension).} \end{aligned}$$

The latter case governs for which the margins of safety are again calculated as for the fin and canister shell; i.e.,

$$\text{M.S.} = \frac{20,000}{(1.15)(13,396)} - 1 = +0.29 \text{ on yield,}$$

$$\text{M.S.} = \frac{30,000}{(1.5)(13,396)} - 1 = +0.49 \text{ on ultimate.}$$

(c) Forward Joint. The clamp band assembly of Figure 2 connects the aft end of the bomb or mine to the forward end of the canister assembly. The external, annual vee groove that is an integral part of the canister forms the forward joint that accepts the clamp band assembly. This joint is located on the canister as shown in Figure 5. The critically stressed area is the cross section A-A of Figure 34 taken through the bottom of the vee groove that is located as shown in Figure 31.

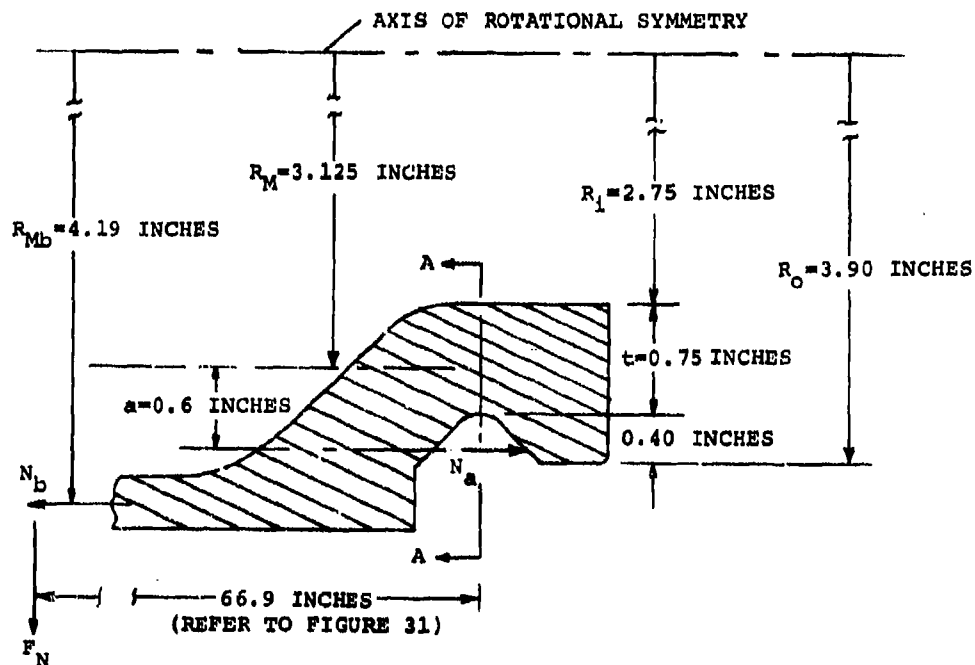


Figure 34. Critical Stressed Area of the Forward Joint

Loading Case 2 governs for which the longitudinal drag and side forces are given on pages 54 and 55, respectively, as $D = 10,250$ pounds and $F_N = 1015$ pounds.

The cross sectional area of the A-A annulus of Figure 34 is

$$A_t = \pi \left[(R_o - 0.40)^2 - R_i^2 \right] = \pi \left[(3.9 - 0.40)^2 - 2.75^2 \right]$$

$$= 14.73 \text{ square inches.}$$

The section modulus at the mean radius of this annulus may be determined from the formulas on page 4.1.5 of Reference 18 as follows:

$$\frac{I}{c} = \frac{\pi}{2} \left(\frac{(R_o - 0.40)^4 - R_i^4}{R_o - 0.40 + R_i} \right) = \frac{\pi}{2} \left(\frac{12.25^2 - 7.56^2}{6.25} \right)$$

$$= 23.34 \text{ cubic inches.}$$

The applied bending moment per Figure 34 is

$$M = 66.9 F_N = (66.9)(1015) = 67,904 \text{ inch pounds.}$$

Hence, the maximum combined average stress on the Section A-A annulus is

$$\sigma_a = \frac{D}{A_t} + \frac{MC}{I} = \frac{10,250}{14.73} + \frac{67,904}{23.34} \quad (34)$$

$$= 696 + 2,909 = 3,605 \text{ pounds per square inch.}$$

A local bending stress must yet be combined with this average stress due to the moment arm, a , indicated in Figure 34. This moment arm is the distance from the neutral axis of Section A-A to the line of action of the resultant bearing force between this forward joint and the mating clamp ring. The neutral axis of a unit width of Section A-A is essentially coincident with the mean radius that, from Figure 34 is

$$R_M = \frac{1}{2} (R_o - 0.4 + R_i) = 3.125 \text{ inches.}$$

Consideration of the compatibility of dimensions between Figures 34 and 35 indicates that the resultant bearing force, N_a , should be placed at half the depth of the vee groove. Therefore, the moment arm is calculated per Figure 34 as

$$a = R_o - \frac{0.40}{2} - R_M = 3.9 - 0.2 - 3.1 = 0.6 \text{ inches}$$

The distributed force on Section A-A is simply

$$\begin{aligned} N_{AA} &= t \sigma_a = (R_o - 0.40 - R_I) \sigma_a = (3.9 - 0.40 - 2.75)(3,605) \\ &= (0.75)(3,605) = 2704 \text{ pounds per inch.} \end{aligned}$$

The distributed bearing force, N_a , is given by equilibrium of longitudinal forces as

$$N_a = \frac{R_M}{R_M + a} N_{AA} = \left(\frac{3.125}{3.725} \right) (2704) = 2269 \text{ pounds per inch.}$$

The local bending moment applied to a unit circumferential length of the Section A-A annulus is then given with reference to Figure 34 as

$$\begin{aligned} M_a &= a \frac{R_M + a}{R_M} N_a = a N_{A-A} = (0.6)(2740) \\ &= 1622 \text{ inch-pounds per inch.} \end{aligned}$$

The corresponding local bending stress is given by the classical flexural formula as

$$\begin{aligned} \sigma_b &= \frac{6M_a}{t^2} = \frac{6(1622)}{(0.75)^2} = (10.667)(1622) \\ &= 17,300 \text{ pounds per square inch.} \end{aligned}$$

The combined stress is

$$\sigma = \sigma_a + \sigma_b = 3,605 + 17,300 = 20,905 \text{ pounds per square inch.}$$

Since this stress is slightly greater than the casting's yield strength ($F_t = 20,000$ pounds per square inch), the extreme outer fibers of Section A-A will yield into the plastic range of the material. However, the entire section will not yield, and a margin of safety on yield may be calculated using theory of plasticity such as presented in Reference 20.

For the rectangular Section A-A, the shape factor per Figure 1a, Page 5.5013 of Reference 20 is,

$$k = 1.5$$

Using this shape factor, the yield and ultimate plastic strength allowables for the 356-T6 aluminum casting are given in Figure 1e, Page 5.5029 of Reference 20, respectively; i.e.,

$$F_{py} = 25,500 \text{ pounds per square inch,}$$

$$F_{pu} = 40,100 \text{ pounds per square inch.}$$

The corresponding margins of safety are:

$$\text{M.S.} = \frac{25,500}{(1.15)(20,905)} - 1 = +0.06 \text{ on plastic yield,}$$

$$\text{M.S.} = \frac{40,100}{(1.5)(20,905)} - 1 = +0.27 \text{ on plastic ultimate.}$$

(5) Clamp Band Assembly

The clamp band assembly is shown in Figure 4. Its load-carrying components are analyzed herein.

(a) Clamp Ring. The clamp ring is a split ring that mates to the vee grooves of the bomb or mine and the forward joint of the Ballute canister. The maximum applied load corresponds to N_a of Figure 34. The component N_a is the longitudinal component of the bearing load between the clamp ring and joint surfaces, and is the only source of combined tensile and bending stresses to be considered. The radial component, N_r , of Figure 35 passes directly through this clamp ring to subject the clamp band to circumferential tension.

In Figure 35, the resultant distributed bearing forces are considered to act at the mean radius of the bearing surfaces. Since these surfaces are machined at 45-degree slope angles with respect to the axis of rotational symmetry, it is obvious that $N_r = N_a$.

From the forward joint analysis,

$$N_a = 2269 \text{ pounds per inch.}$$

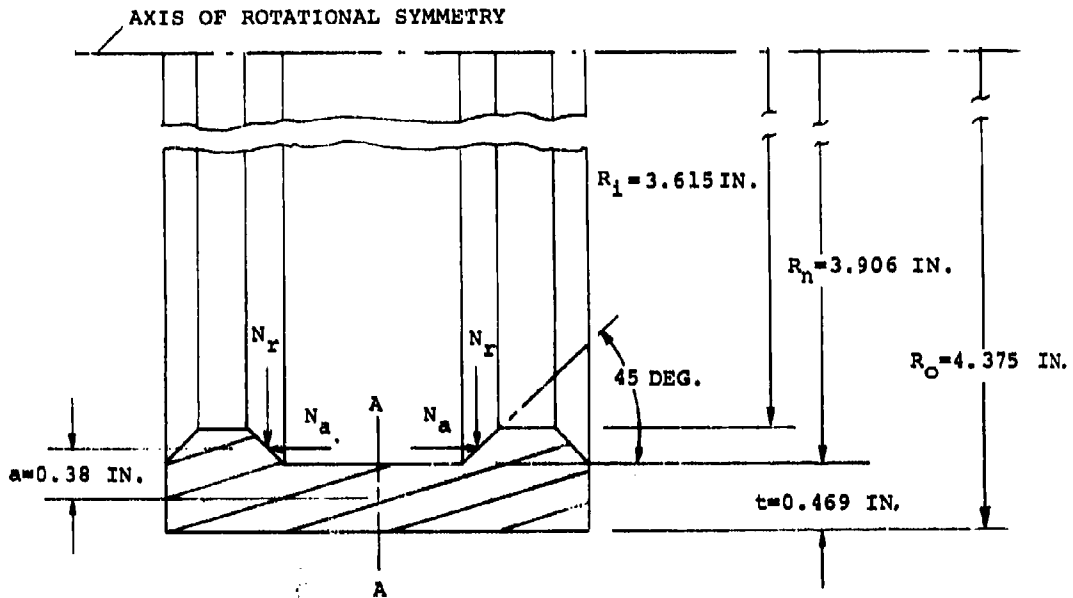


Figure 35. Critical Stressed Area of the Clamp Ring

The tensile and bending stresses on Section A-A of Figure 35 are calculated as follows:

$$\begin{aligned}
 a &= \frac{1}{2} (R_o + R_n) - \frac{1}{2} (R_n + R_i) = \frac{1}{2} (R_o - R_i) \\
 &= \frac{1}{2} (4.375 - 3.615) = 0.38 \text{ inches}
 \end{aligned}$$

$$t = R_o - R_n = 4.375 - 3.906 = 0.469 \text{ inches.}$$

The tensile stress is

$$\sigma_a = \frac{N_a}{t} = \frac{2269}{0.469} = 4,838 \text{ pounds per square inch.}$$

The bending stress is

$$\sigma_b = \frac{6a N_a}{t^2} = \frac{6 (0.38) (2269)}{(0.469)^2}$$
$$= 23,515 \text{ pounds per square inch.}$$

The combined stress is

$$\sigma = \sigma_a + \sigma_b = 4,838 + 23,515$$
$$= 28,353 \text{ pounds per square inch.}$$

The ring is machined from 4142-H alloy steel tubing that is heat treated to an ultimate tensile strength of $F_{tu} = 140,000$ pounds per square inch. The margin of safety is then

$$\text{M.S.} = \frac{140,000}{(1.5)(28,353)} - 1 = +2.29.$$

(b) Clamp Band. The basic circumferential tension in the clamp band is due to two of the distributed radial loads denoted by N_r in Figure 35. $2N_r$ is the maximum radial load due to the combined drag plus side loadings of Case 2. Therefore, this load is not distributed uniformly around the circumference of the band but is primarily distributed as a cosine function to be compatible with the M_c/I stress term of Equation 34. In fact, tracing back the calculations that lead to $N_r = N_a = 2269$ pounds per inch show that $2N_r$ may be divided into a uniform distribution and into a cosine distribution that are in direct proportion to the two right-hand terms of Equation 34, respectively. These are calculated below and are shown in the two free-body diagrams in the plane of the clamp band of Figure 36.

$$N_{ru} = \text{the uniformly distributed component of } 2 N_r$$
$$= 2 \left(\frac{696}{3,605} \right) (2269) = 876 \text{ pounds per inch.}$$

$$N_{rc} = \text{the maximum value of the cosine distribution of } 2 N_r$$
$$= 2 \left(\frac{2,909}{3,605} \right) (2269) = 3662 \text{ pounds per inch.}$$

From Figure 35, these loads act on the radius

$$\frac{1}{2} (R_n + R_1) = \frac{1}{2} (3.906 + 3.615) = 3.761 \text{ inches.}$$

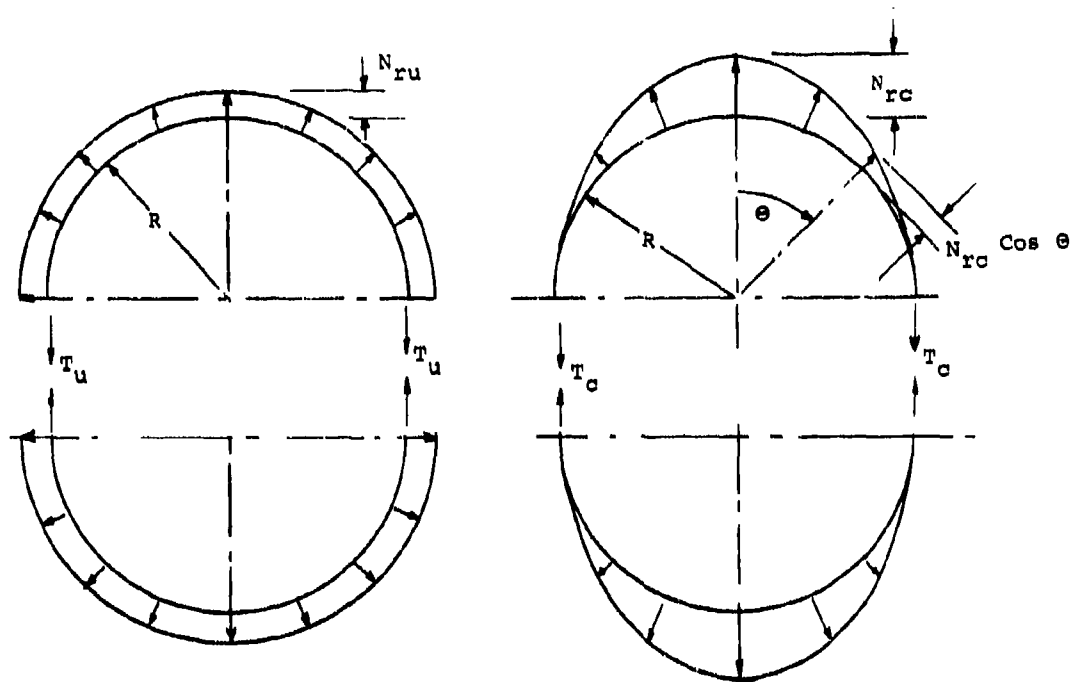


Figure 36. Free Body Diagrams in the Plane of the Clamp Band

The thickness of the clamp band is 0.08 inch. It is located around the clamp ring per Figures 4 and 35 so that its mean radius is

$$R = \left(R_0 + \frac{0.08}{2} \right) = 4.375 + 0.04 = 4.415 \text{ inches}$$

Transfer of the above distributed forces to the mean circumference of the band yields the reduced values of

$$N_{ru} = \left(\frac{3.761}{4.415} \right) (876) = 746 \text{ pounds per inch,}$$

$$N_{rc} = \left(\frac{3.761}{4.415} \right) (3662) = 3120 \text{ pounds per inch.}$$

Equilibrium of forces in Figure 36 yields the maximum circumferential tension in the clamp band as follows:

$$T_u = R N_{ru} = (4.415)(746) = 3,294 \text{ pounds.}$$

$$T_c = R N_{rc} \int_0^{\pi/2} \cos^2 \theta d\theta = \frac{\pi}{4} R N_{rc} = \frac{\pi}{4} (4.415)(3120)$$

$$= 10,819 \text{ pounds.}$$

The total maximum tension is therefore

$$T = T_u + T_c = 3,294 + 10,819 = 14,113 \text{ pounds} \quad (35)$$

The critical section of the clamp band is located at the attachment to the index block of Figure 4. At this location, there are two 0.375-inch diameter holes through the 2.66-inch wide band. The minimum net tensile area of the 0.08-inch thick band is

$$A_t = [2.66 - (2)(0.375)] (0.08) = 0.1528 \text{ square inches.}$$

The applied tensile stress and the ultimate margin of safety for the 4130 steel band as heat treated to an ultimate tensile strength of $F_{tu} = 136,000$ pounds per square inch are, respectively,

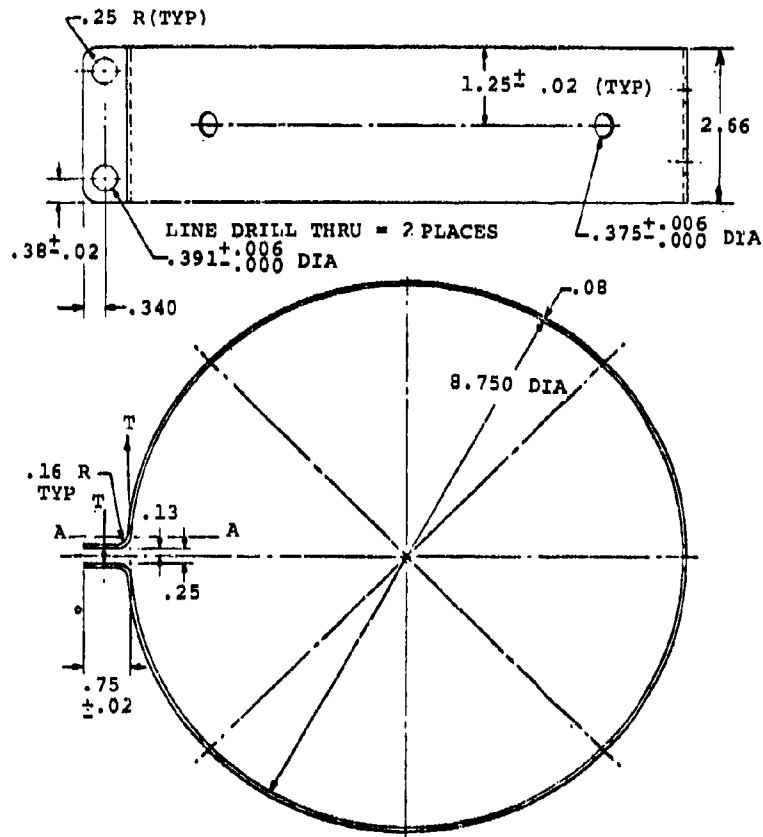
$$\sigma = \frac{T}{A_t} = \frac{14,113}{0.1528} = 92,363 \text{ pounds per square inch,}$$

$$M.S. = \frac{136,000}{(1.5)(92,363)} - 1 = -0.02.$$

This slightly negative margin shows that the index block attachment area of the clamp band is the most critical area of the entire Ballute canister assembly.

A stress check of the bend in the clamp band, where the two MS 24678-47 connecting screws of Figure 4 are located, is presented below. The first calculation shows the excessive stresses that would result if the three gusset plates were to be omitted. The second calculation considers the area to be reinforced with the gussets of the present design. This area is detailed in the free bodies of Figures 37 and 38. The applied load in both cases is given by Equation (35); i.e.,

$$T = 14,113 \text{ pounds.}$$



ALL DIMENSIONS ARE IN INCHES

Figure 37. Free Body of Bend in the Clamp Band, Gussets Omitted

The combined tensile and bending stress on Section A-A of Figure 37 is

$$\sigma = \frac{T}{A_t} + \frac{6M}{bt^2}$$

where,

T = 14,113 pounds

t = thickness of the band = 0.08 inch

b = width of the band = 2.66 inches

A_t = tensile area = $bt = (0.08)(2.66) = 0.2128$ square inches

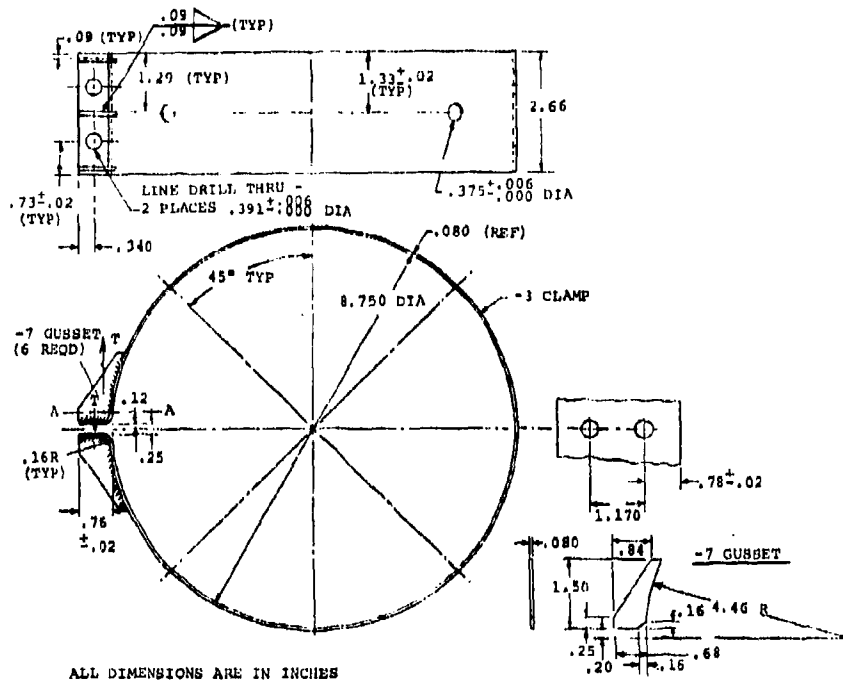


Figure 38. Free Body of Bend in the Clamp Band, Gussets Included

M = the applied bending moment, that from the dimensions of Figure 37 is

$$M = (0.75 + 0.02 - 0.340 - \frac{0.08}{2}) T \quad (36)$$

$$= (0.39)(14,113) = 5,504 \text{ inch-pounds}$$

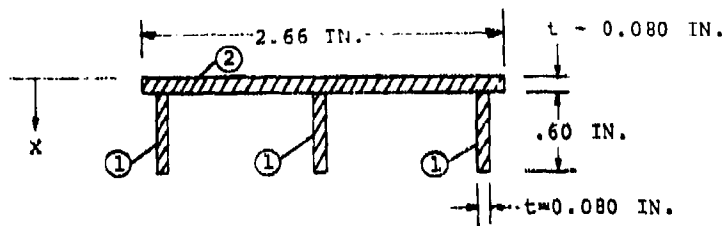
Therefore,

$$\sigma = \frac{14,113}{0.2128} + \frac{6(5,504)}{2.66(0.08)^2} = 66,320 + 1,938,680$$

$$= 2,005,000 \text{ pounds per square inch.}$$

Next, consider the gusseted design of Figure 38 and again calculate the combined stresses across Section A-A of this figure. This area is shown in Figure 39 where the area, ΣA_t , centroidal distance, \bar{x} , and moment of

SECTION A-A of Figure 38



| | ITEM | A_t | x | $A_t x$ | $A_t x^2$ | I_o |
|-----|---------------|-------|-------|---------|-----------|---------|
| (3) | 0.080 x 0.60" | 1 | 0.144 | 0.040 | 0.00376 | 0.00023 |
| (1) | 2.66 x 0.080" | 2 | 0.213 | 0.380 | 0.08094 | 0.00011 |
| | Σ | - | 0.357 | 0.08670 | 0.03099 | 0.00443 |

$$\bar{x} = \frac{\Sigma A_t x}{\Sigma A_t} = \frac{0.08670}{0.357} = 0.243 \text{ inches}$$

$$I = \Sigma A_t x^2 + \Sigma I_o - \bar{x} \Sigma A_t x$$

$$= 0.03099 + 0.00443 - (0.0867)(0.243)$$

$$= 0.01435 \text{ inch to the fourth power}$$

Figure 39. Section Properties of the Gusseted Band Area

inertia, I , are calculated. The distance from the centroidal axis to the extreme fiber on the tension side of the section is taken from Figure 39 as

$$c = 0.60 + 0.08 - \bar{x} = 0.68 - 0.243 = 0.437 \text{ inches.}$$

The applied tension is given by Equation(35). This acts at the centroidal distance of the cross section and is reacted at the screw centerlines. Hence, per the dimensions of Figures 38 and 39, the applied bonding moment is

$$M = (0.76 + 0.02 - 0.340 - \bar{x}) T$$

$$= (0.44 - 0.243) (14,113) = 2,780 \text{ inch-pounds.}$$

The desired combined tensile and bending stress on Section A-A of Figure 38 is, therefore,

$$\begin{aligned}\sigma &= \frac{T}{\Sigma A_t} + \frac{Mc}{I} = \frac{14,113}{0.357} + \frac{(2,780)(0.437)}{0.01435} \\ &= 39,532 + 84,659 = 124,191 \text{ pounds per square inch.} \quad (37)\end{aligned}$$

This stress level requires that the plastic range of the material's load-elongation properties be considered in order to calculate an ultimate positive margin of safety. As was previously used in the analysis of the forward joint, the method of Reference 20 is applied.

The shape factor for the section of Figure 39 is given by the equation on Page 5.5013 of the reference as

$$k = \frac{2cQ}{I} = \frac{3t}{I}c^3 = \frac{3(0.08)}{0.01435}(0.437)^3 = 1.40$$

The 4130 steel alloy is heat treated to an ultimate tensile strength of $F_{tu} = 136,000$ pounds per square inch. The corresponding ultimate value of the plastic bending stress, i.e. F_{bu} is taken from Figure 1f, Page 5.5030 of Reference 20 as

$$F_{bu} = 186,000 \text{ pounds per square inch.}$$

For the combined stress condition, the interaction method on Page 5.5023 of the reference is applied to give the margin of safety.

$$M.S. = 1 - \frac{F.S. \sigma_b}{F_{bu}} - \left(\frac{F.S. \sigma_a}{F_{tu}} \right)^n$$

(Refer to Figure 1d, Page 5.5028 of Reference 20)

where:

- F.S. = the ultimate factor of safety = 1.5
- σ_a = 39,532 pounds per square inch (Equation 37)
- σ_b = 84,659 pounds per square inch (Equation 37)
- n = an exponent given in Figure 1c, Page 5.5027 of Reference 20

In order to obtain the above value for n in the referenced figure, the following two parameters must be determined:

$\gamma = 0.93$ for the steel with $F_{tu} = 136,000$ pounds per square inch as interpolated in the table on Page 5.5023 of Reference 20.

$$\frac{\Sigma A_t \bar{x}}{2Q} = \frac{\Sigma A_t \bar{x}}{3 t c^2} = \frac{(0.357)(0.243)}{3 (0.08)(0.437)^2} = 1.89.$$

(Refer to Figure 39)

Entering these two values in the referenced figure gives

$$n = 1.74.$$

Therefore,

$$\begin{aligned} \text{M.S.} &= 1 - \frac{(1.5)(84,659)}{186,000} - \left[\frac{(1.5)(39,532)}{136,000} \right]^{1.74} \\ &= 1 - 0.683 - (0.436)^{1.74} = +0.08. \end{aligned}$$

(c) MS 24678-47 Screws. These two screws connect the terminal ends of the clamp band and are located between the three gussets of Figure 38. The screws are shown on the clamp band assembly of Figure 4.

The ultimate tensile strength per each of the two screws is given in the MS Standard as

$$P_u = 13,800 \text{ pounds per screw.}$$

The applied load per screw is one-half of the circumferential tension of Equation(35); i.e.,

$$P = \frac{1}{2} (14,113) = 7,057 \text{ pounds per screw.}$$

Therefore, the ultimate margin of safety is

$$\text{M.S.} = \frac{P_u}{(\text{F.S.}) P} - 1 = \frac{13,800}{(1.5)(7,057)} - 1 = +0.30.$$

SECTION VI
VIBRATION TESTS

1. GENERAL

Sinusoidal vibration tests were conducted to determine whether the MK82 Ballute retarder system could withstand the vibrational environment in subsequent flight tests. The retarder system tested met the requirements, and no damage or deterioration of the retarder system occurred as a result of these tests.

2. TEST PROCEDURE

a. Introduction

Vibration tests were conducted in accordance with MIL-STD-810B, Method 514.1, Procedure 1, Part I, Curve G. These tests consisted of a vibration survey at reduced input levels, resonant dwells, and cycling tests. These tests were conducted in each of the three mutually perpendicular axes. A maximum acceleration level of 14-g was used for tests in lieu of 15-g. This reduction of test level is permitted by MIL-STD-810B as a result of the 62-pound weight of the retarder system. A total test time of 3 hours per axis of test was performed.

Instrumentation in the form of a triaxial accelerometer was placed at the aft end of the retarder system near the root of a fin. One accelerometer was placed on each of two transverse fins. Figure 40 illustrates the instrumentation.

The vibration input control was at the forward end of retarder system adjacent to the interface of the vibration adapter plate. Oscillographic recordings were made of input control and accelerometer outputs.

b. Transverse Axis Number 1 Tests

A vibration adapter plate was attached to an auxiliary hydrostatic bearing vibration table. The MK82 Ballute retarder system was attached to the adapter plate by means of the clamp assembly.

The axis of applied vibration was parallel to one set of fins and was designated as Transverse Axis Number 1. Figures 40 and 41 show the installation.

c. Transverse Axis Number 2 Tests

The MK82 Ballute retarder system was rotated approximately 90 degrees on the adapter plate such that the applied vibration was in the other transverse axis which was designated as the Transverse Axis Number 2. This installation is shown in Figures 42 and 43.

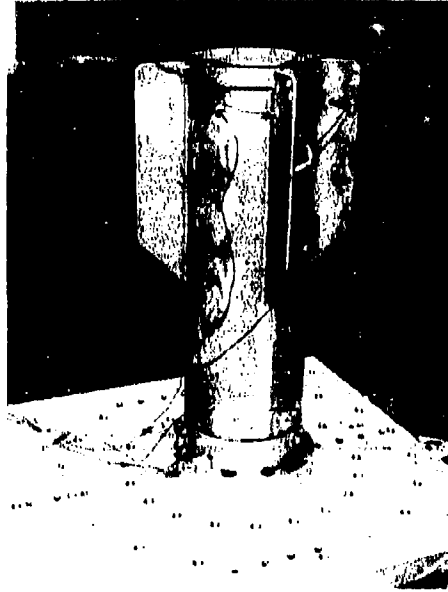


Figure 40. Vibration Instrumentation and Transverse Axis Number 1 Installation

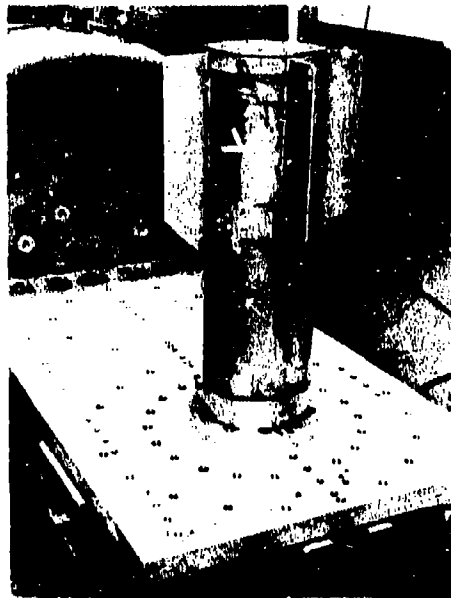


Figure 41. Transverse Axis Number 1 Installation

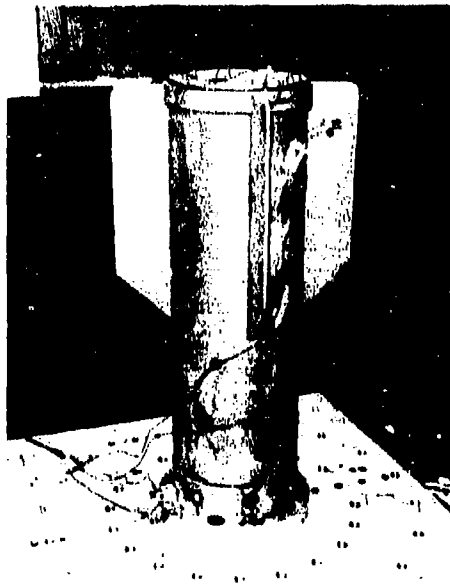


Figure 42. Transverse Axis Number 2 Installation.

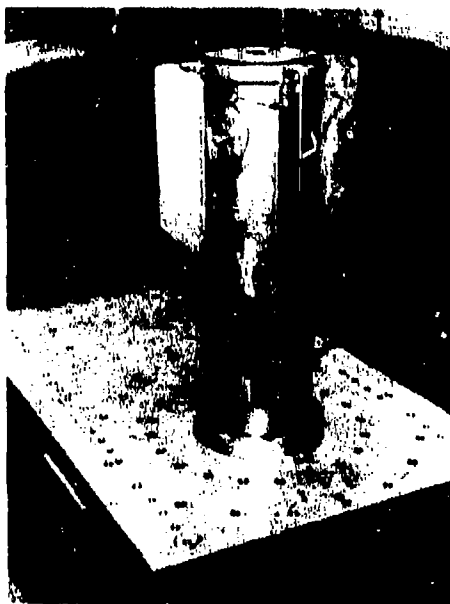


Figure 43. Transverse Axis Number 2 Installation

d. Longitudinal Axis Tests

The adapter plate was removed from the auxiliary hydrostatic bearing vibration table and reattached directly to the vibration exciter head. The MKS2 Ballute retarder system was then attached to the vibration adapter plate. Figure 44 shows the longitudinal axis installation.

3. TEST RESULTS

All test equipment used was maintained and calibrated in accordance with MIL-C-45662A, dated 9 February 1962. A list of equipment used is presented in Table V.

Visual examinations were performed upon completion of each dwell test and upon completion of cycling tests. There were no indications of damage or deterioration of the retarder system as a result of vibration tests. During Transverse Axis Number 1 tests, a discrepancy was noted on the clamp ring, and the results are documented in Transverse Axis Number 2 test results.

a. Transverse Axis Number 1 Tests

During the reduced input survey vibration tests (10 g input), the monitor accelerometers on the fins were relocated to 1/3 of the distance from the root of the fin to the tip. This change was necessitated due to high ($700 \pm g$) levels recorded on fins tips at approximately 900 Hz which would destroy instrumentation. All vibration test levels recorded for the fins will reflect the resonant values from this new attachment point.

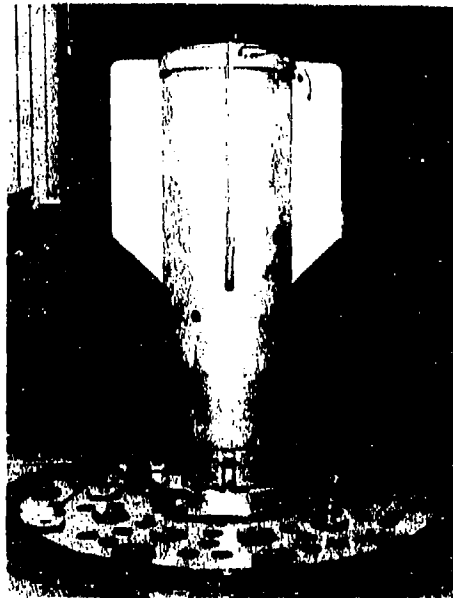


Figure 44. Longitudinal Axis Installation

TABLE V. VIBRATION TEST EQUIPMENT

| Item No. | Equipment Name | Manufacturer | Model Number | Serial Number | Range | Accuracy | Calibration Date and Cycle |
|----------|-----------------------------|----------------|----------------|--|-------------------|------------------------------|-------------------------------------|
| 1 | Vibration System | MB Mfg. Co. | C-210 | L6554 | 20,000 Force Lb | N/A | 3-6-72 |
| 2 | Accelerometers Control (2) | Endevco | 2213 | 6840 8820 | 2 Hz 5K Hz | ±2% 0-1000G | 3-3-72 4 months 4-13-72 3 months |
| 3 | Amplifiers (5) | Unholtz-Dickie | CVA605 RM06 | L7176 L7179 L7181 L7186 L7187 | 0-1000G | ±3% 5 Hz to 10 K Hz | 5-11-72 3 months |
| 4 | Accelerometers, Monitor (5) | Endevco | 2226C | TF38 TF71 UJ13 TG51 UN14 | 0-1000G | ±2% 5 Hz-10K Hz | 3-3-72 4 months |
| 5 | Oscillograph | Honeywell | 1012 | L3658 | 1-160 In. /Sec | ±2% | 4-17-72 3 months |
| 6 | Galvanometers (6) | Honeywell | M-5000 | 52015 18333 153494 153533 153532 1F321487 | DC-3K Hz | 5% | 9-16-72 9 months |

Four resonant frequencies were noted during resonance search tests and are listed below:

- (1) 110 to 115 Hz. - This is the first bending mode of the entire system. The resonant frequency started at 115 Hz and shifted to 110 Hz after 12 minutes of dwell tests. This was due to slight wearing of the clamp ring against the fixture and the Ballute canister.
- (2) 479 Hz. - This resonant condition was noted on Pickup No. 4 Transverse Axis No. 2 fin and appears to be a bending mode of fin. At T + 8 minutes the resonant frequency was shifted to 408 Hz. There is no known reason for the frequency change. No damage was noted.
- (3) 920 Hz. - This condition was noted on the same fin as resonance No. 2. A Q (transmissibility at resonance) of 8.6 was recorded. This is possibly a bending mode of the fin.
- (4) 1106 Hz. - A 100 g level was recorded on Transverse Axis No. 2 fin. Upon completion of cycling tests and each of the dwell tests, visual examinations were made to determine whether there was any damage.

Two hours of dwell tests, 30 minutes at each of the above frequencies and one hour of cycling, from 5 to 2000 to 5 Hz in 20-minute sweeps, were performed. These examinations revealed no damage to case or contents that could be seen without complete disassembly.

Table VI lists the recorded values obtained during dwell tests.

b. Transverse Axis Number 2 Tests

During the resonance search tests (3g), the recorded outputs of the monitor accelerometer channels revealed a resonance at 70 Hz with much impact loading.

The clamp assembly was removed, and inspection revealed the clamp ring was touching in only two areas.

The clamp ring was machined so that it would mate the Ballute canister to the vibration fixture more effectively.

The resonance search was repeated and the four resonant frequencies chosen from this are listed below.

- (1) 125 Hz - The retarder system is in a bending mode. No change in resonant frequency was recorded during tests.
- (2) 959 Hz - This was a resonant condition for the Transverse Axis Number 1 fin and for the Ballute canister at the root of the fin. A 200 g level was recorded on Channel No. 5.
- (3) 1199 Hz - This was a resonant condition for the Transverse Axis Number 1 fin in bending. A 190 g output level was recorded.
- (4) 1897 Hz - This was a local resonance at the aft end of the Ballute canister near the root of a fin. Channel No. 2 recorded a level of 91 g.

Four resonance dwells, each of 30 minutes in duration, and three cycles each of 20 minutes in duration, were performed for a total test time of 3 hours.

The visual examination after each dwell test and after the cycling tests revealed no damage or deterioration as a result of vibration tests.

Table VII lists the data recorded during dwell tests.

c. Longitudinal Axis Tests

The resonance search revealed only one resonant frequency at 954 Hz. This appeared to be a compression mode along the longitudinal axis with an output response level of 120 g. A 30-minute resonant dwell was run at this frequency.

TABLE VI. TEST DATA - TRANSVERSE AXIS NUMBER 1

| Frequency (Hz) | Input Level (G) | Aft End of Ballute Canister | | | Fins | |
|----------------|-----------------|-----------------------------|----------------------|------------------|----------------------|----------------------|
| | | Transverse No. 1 (G) | Transverse No. 2 (G) | Longitudinal (G) | Transverse No. 2 (G) | Transverse No. 1 (G) |
| 115 | 14 | 50 | 6 | 18 | 60 | 18 |
| 109 | 14 | 50 to 70 * | 6 to 10 * | 18 to 27 * | 50 to 70 * | 20 to 40 * |
| Note 1 | | | | | | |
| 448 | 14 | 7.5 | 12 | 6.5 | 45 | 54 |
| 408 | 14 | 8 | 13 | 7 | 54 | 48 |
| Note 2 | | | | | | |
| 920 | 14 | 50 | 24 | 40 | 130 | 100 |
| 1106 | 14 | 24 | 21 | 55 | 100 | 45 |

* Two frequencies modulating against each other only minimum and maximum values recorded.

Note 1 - The resonant frequency started at 115 Hz and shifted to 110 Hz after 12 minutes of dwell testing. The remaining portion of test period was conducted at the new (109 Hz) resonant frequency.

Note 2 - The original resonant frequency of 448 Hz shifted to 408 Hz after 8 minutes of testing. Test period concluded at new frequency.

TABLE VII. TEST DATA - TRANSVERSE AXIS NUMBER 2

| Frequency (Hz) | Input Level (G) | Aft End of Ballute Canister | | | Fins | |
|----------------|-----------------|-----------------------------|----------------------|------------------|----------------------|----------------------|
| | | Transverse No. 1 (G) | Transverse No. 2 (G) | Longitudinal (G) | Transverse No. 2 (G) | Transverse No. 1 (G) |
| 125 | 14 | 40 - 70 * | 50 - 120 * | 40 - 80 | 20 - 30 * | 50 - 100 * |
| 938 | 14 | 15 | 60 | 27 | 100 | 180 |
| 1199 | 14 | 8 | 35 | 18 | 55 | 190 |
| 1897 | 14 | 17 | 91 | 18 | 25 | 20 |

* Two frequencies modulating against each other. Both minimum and maximum values were recorded

Two and one-half hours of cycling, with a 20-minute duration per cycle, were then performed to comply with the three-hour vibration requirement.

The post-dwell and cycling visual examinations revealed no damage or deterioration to the MK82 Ballute retarder system as a result of vibration tests.

Table VIII lists the data obtained during the dwell test.

4. CONCLUSIONS

The results of the visual inspections and data gathered indicate that the MK82 Ballute retarder system will withstand the vibration environment which was simulated.

TABLE VIII. TEST DATA - LONGITUDINAL AXIS

| Frequency (Hz) | Input Levels (g) | Aft End of Ballute Coaster | | | Fins | |
|-------------------|------------------------|----------------------------|-------------------------|---------------------|-------------------------|-------------------------|
| | | Transverse No. 1 (g) | Transverse No. 2 (g) | Longitudinal (g) | Transverse No. 2 (g) | Transverse No. 1 (g) |
| 893 | 14 | 80 | 30 | 120 | 60 | 70 |

SECTION VII

CONCLUSIONS AND RECOMMENDATIONS

Conclusions and recommendations resulting from this advance development effort follow:

1. CONCLUSIONS

- (a) The estimated static margin of the MK82/Ballute canister is equal to or greater than the MK82/MAU-93 for most Mach numbers of concern.
- (b) The variation of static margin with roll attitude cannot be predicted either analytically or by comparison of available wind tunnel data.
- (c) The dynamic stability cannot be predicted due to nonavailability of wind tunnel and flight test data.
- (d) Results of the structural analysis indicate that the developed system is structurally adequate for subsequent flight testing.
- (e) Results of the vibration tests indicate that the system can withstand the vibration environment of subsequent flight testing.

2. RECOMMENDATIONS

- (a) A wind tunnel test program is recommended to determine the following:
 - (1) Effect of roll attitude on static stability.
 - (2) Linear and nonlinear static aerodynamic characteristics.
 - (3) Dynamic stability characteristic variations with Mach number and angle of attack.
 - (4) Effect of the tail planform on static and dynamic stability.
- (b) A static load test program is recommended to determine the following:
 - (1) Structural limits of the clamp and canister assemblies.
 - (2) Minimum nylon strength required for Ballute construction.

REFERENCES

1. "Trajectory Control of Stores," First Quarterly Report, GER-15234, Goodyear Aerospace Corporation, 1 April 1971.
2. Pitts, W. C., Nielsen, J. N., and Kaattari, G. E.; "Lift and Center of Pressure of Wing-Body-Tail Combinations at Subsonic, Transonic and Supersonic Speeds," NACA TR1307, 1957.
3. Asper, M., "Parametric Lift and Center of Pressure Charts for Low Aspect Ratio Fin-Body Combinations Through a Mach Number Range of 0.4 to 3.5," Memorandum Report SU-12445, Goodyear Aerospace Corporation, May 1965.
4. Asper, M., and Byers, P. D.; "Transonic Wind Tunnel Tests of a 0.50-Scale Model of the Hard-Structures Munition," GER-13629, Goodyear Aerospace Corporation, Akron, Ohio, January 1968.
5. Turk, R. A.; "Pressure Measurements on Rigid Model of Ballute Decelerator at Mach Number from 0.56 to 1.96," NASA TND-3545, August 1966.
6. Richenau, D. E.; "Deployment of Inflatable Decelerator Attached to an M-117 Bomb at Mach Numbers from 0.55 to 1.40," AEDC-TR-69-40, April 1969.
7. Sherburne, P. A.; "Low-Speed Wind Tunnel Test of Several Rigid Ballute Models," GER-14306, Goodyear Aerospace Corporation, March 1969.
8. Caldwell, R. L.; "Transonic Wind Tunnel Investigations of Ballute-Stabilized Bomb Configuration," AEDC-TR-71-8, January 1971.
9. Piper, W. D., and DeMeritte, F. J.; "Summary of the NOL Investigations to Date of the Aerodynamic Characteristics of the Navy Low-Drag Bomb," NAVORD Report 5679, February 1960.
10. Regan, F. T., et al; "Static Wind-Tunnel Tests of the Mk 82 Free-Fall Store with Two Modified Stabilizers," NOLTR 69-217, December 1969.
11. Sheeter, H. H.; "Transonic Wind Tunnel Investigations of the Influence of Spherically-Blunted, Tangent-Ogive Noses on the Drag and Stability of a Body of Revolution." GER-14876, Goodyear Aerospace Corporation, June 1970.
12. Eaton, P. T.; "A Method for Predicting the Static Aerodynamic Characteristics of Low-Aspect-Ratio Configurations", David Taylor Model Basin (DTMB) Report 2216, June 1966.
13. Homen, M. L.; "Static Stability Characteristics of the M-117 Bomb at Mach Numbers from 0.60 to 1.40 with Three Tail Fin Configurations," AEDC-TR-68-162, July 1968.
14. DuPont, "Stress-Strain Properties of DuPont Nylon," Bulletin Number, N-180, October 1964, E. I. DuPont De Nemours and Co., Textile Fibers Department, Wilmington, Delaware.

REFERENCES (Concluded)

15. Timoshenko, S., and Woinowsky-Krieger, S.; "Theory of Plates and Shells," Second Edition, 1959. McGraw-Hill Book Company, Inc., New York, N. Y.
16. MIL-HDBK-5B, "Military Standardization Handbook, Metallic Materials and Elements for Aerospace Vehicle Structures," 1 September 1971. Department of Defense, Washington, D. C.
17. Roark, R. J., "Formulas for Stress and Strain," McGraw-Hill Book Company, 1954, New York, N. Y.
18. "Weight Engineers Handbook," Revised, December 1968, Society of Aeronautical Weight Engineers, Inc., P. O. Box 60024 Terminal Annex, Los Angeles, California, 90054.
19. "Moments, Shears and Axial Loads in Rings," SM 10103, Goodyear Aerospace Corporation.
20. "Structures Design Manual," Revision J, November 3, 1958, Goodyear Aerospace Corporation, Akron, Ohio.

UNCLASSIFIED

Security Classification

DOCUMENT CONTROL DATA - R & D

(Security classification of title, body of abstract and indexing annotation must be entered when the overall report is classified)

| | |
|--|--|
| 1. ORIGINATING ACTIVITY (Corporate author) Goodyear Aerospace Corporation 1210 Massillon Road Akron, Ohio 44315 | 2a. REPORT SECURITY CLASSIFICATION UNCLASSIFIED |
| | 2b. GROUP |

3. REPORT NUMBER
MK82 BALLUTE RETARDER SYSTEM

4. REPORT DATE
Final Report, 1 Jan 1972 to 30 Sep 1972

5. AUTHOR(S)
N. T. Karaffa, A. C. Debiach, S. A. Wainberg, J. F. ...

6. PERIODICITY
Sep 1972

7a. TOTAL NO. OF PAGES
96 pgs

7b. NO. OF ILLS
20

8. COLLECTOR(S)
E08635-72-C-0096

9. ORIGINAL REPORT NUMBER(S)
GER-15693

10. PROJECT NUMBER
AF-1559

11. OTHER REPORT NUMBER(S) (Any other numbers that may be assigned this report)
AFATL TR-72-179

12. TASK NO.
13

13. WORK UNIT NO.
001

14. DISTRIBUTION STATEMENT
Distribution limited to U. S. Government agencies only; this report documents test and evaluation; distribution limitation applied September 1972. Other requests for this document must be referred to the Air Force Armament Laboratory (DLJC), Eglin Air Force Base, Florida 32542.

15. SUPPLEMENTARY NOTES
Available in DDC

16. SPONSORING MILITARY ACTIVITY
Air Force Armament Laboratory
Air Force Systems Command
Eglin Air Force Base, Florida 32542

17. ABSTRACT
Two retarder systems for the MK82, utilizing ram-air inflated Ballutes, were designed, developed, fabricated, and tested. One system was designed for MK82 mine application and the other system for MK82 general purpose bomb application. Ballistic characteristics of the MK82 general purpose system in the low drag mode are to be comparable to the MK82/MAU-93 and in the high drag mode to be comparable to the MK82/MK15. The system is to function in association with the MAU-146 timer, FMU-54 fuze, and ATU-35 drive assembly. Basic technical disciplines presented herein are design, aerodynamic analysis, and structural analysis. Vibration test results are also presented. Both types of system were delivered for flight testing and system feasibility testing by the Armament Development and Test Center.

156 800 ✓

mk

UNCLASSIFIED

Security Classification

| 14 KEY WORDS | LINK A | | LINK B | | LINK C | |
|---|--------|----|--------|----|--------|----|
| | ROLE | WT | ROLE | WT | ROLE | WT |
| MK82 Bomb Retarder System General Purpose Bomb MAU-93 Fin Ballute Retarder System MAU-146B Timer ATU-35 Drive Assembly MK15 Fin FMU-54 Fuze Mine | | | | | | |

UNCLASSIFIED

Security Classification